

Can Temperature-Programmed Techniques Provide the Gold Standard for Carbon Surface Characterization?

Felix Herold,* Jan Gläsel, Bastian J. M. Etzold, and Magnus Rønning*

Cite This: *Chem. Mater.* 2022, 34, 8490–8516

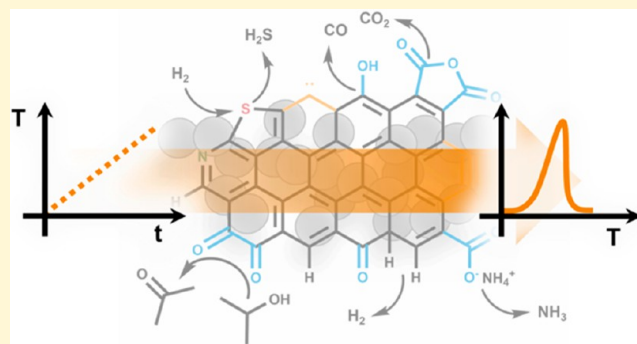
Read Online

ACCESS |

Metrics & More

Article Recommendations

ABSTRACT: Due to their chemical and thermal stability, electrical conductivity, and high specific surface areas, nanocarbons and porous carbon materials have found use in numerous key applications within the current transition of energy and raw-material sources. Since all these applications rely on multiphase interactions between the carbon surface and surrounding solid, liquid, or gaseous phases, carbon surface chemistry is elevated to a critical factor of influence. However, the characterization of carbon surface chemistry is notoriously complex, involving carbon defect sites and chemically similar heteroatom species in a wide range of different binding states and chemical environments. Due to this high degree of complexity, a comprehensive characterization of carbon surface species and reactivity is a major challenge for which there is no analytical “silver bullet” but is fundamental to the rational development of advanced functional carbon materials. In this context we would like to highlight the potential of temperature-programmed techniques (TPX) for carbon surface analytics, which benefit from widely available, easy-to-handle equipment and offer information on the identity, quantity, and reactivity of surface species. Hence, this article reviews the state of the art concerning temperature-programmed techniques for carbon surface characterization, focusing not only on the qualitative and quantitative analysis of carbon surface species but also on the unique ability of temperature-programmed methods to assess carbon surface reactivity. In this context, progress made so far in temperature-programmed desorption, temperature-programmed reduction, and temperature-programmed surface reactions is discussed, highlighting pitfalls and gaps in knowledge. Based on this foundation, strategies for the further development of temperature-programmed methods for carbon surface analysis are proposed, aiming to establish TPX as the future gold-standard in carbon surface characterization.



1. INTRODUCTION

Functional carbon materials play a key role in sustainable energy storage and conversion processes,^{1,2} gas separation and storage,^{3,4} water purification,⁵ and catalysis.^{6–9} This wide field of application for functional carbon materials can be attributed to a combination of favorable properties such as porosity, high electric conductivity, broad thermal and chemical stability, and tunable surface chemistry. The character of a functional carbon material is determined by the interplay of texture (specific surface area and pore size distribution), microstructure (hybridization and crystallinity) and surface chemistry, which is in turn is defined by the presence or absence of defect sites or heteroatoms. Since multiphase processes that rely on the interaction of solid, gaseous, liquid, or dissolved species with the carbon surface represent the lion’s share of applications, carbon surface chemistry and reactivity play a fundamental role in the design and performance of functional carbon materials. For example, this point is perfectly illustrated by membrane electrode assemblies in polymer–electrolyte fuel cells, where functional carbon materials stand in direct contact with solid

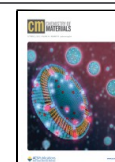
(ion-conducting polymer and Pt electrocatalysts), liquid (H₂O), and gaseous (H₂, O₂, and H₂O) phases. These functional carbons are required to perform a wide variety of tasks simultaneously, ensuring electrical contact, the dispersion and stability of the Pt catalyst, and the transport of reactants to and the removal of reaction products from the catalytically active sites.^{10,11}

This multifunctionality of carbonaceous materials is in large part enabled by the tunable, rich surface chemistry that results from a particularly high diversity of surface species. However, the downside of this rich carbon surface chemistry is its highly challenging analysis, since the diversity of chemically similar

Received: August 10, 2022

Revised: September 14, 2022

Published: September 26, 2022



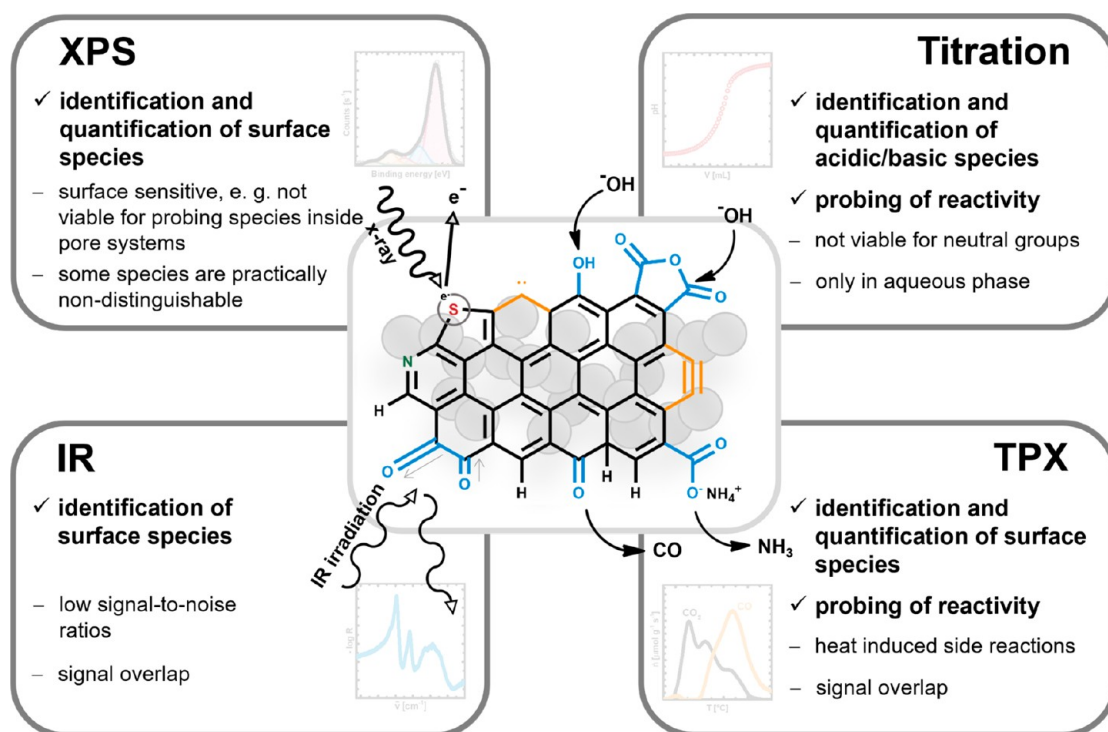


Figure 1. The high diversity of similar carbon surface species, for example, oxygen surface groups, presents a challenge to any individual analysis method, requiring the combination of multiple analysis techniques in order to obtain a meaningful qualitative and quantitative assessment of carbon surface species.

carbon surface species ultimately hampers any attempt at qualitative and quantitative analysis. In this sense, Figure 1 illustrates the lack of any analytical “silver bullet”, with X-ray photoelectron spectroscopy (XPS), titration (potentiometric titration and Boehm titration), temperature-programmed techniques (TPX), and infrared (IR) spectroscopy being the most common analytical tools. Consequently, the comprehensive analysis of carbon surface species and reactivity can only be achieved by combining several methods. However, it is also implied that continued investment in the development of each individual method offers the potential to significantly facilitate the complicated task of characterizing the surfaces of carbons and also provides new pathways toward previously inaccessible information.

In this contribution, we want to make the case for the further development of temperature-programmed analysis techniques (TPX), as we believe that a high return of investment can be expected. This expectation is based mainly on the unique ability of TPX methods to provide both qualitative and quantitative analyses of surface species while further providing access to information on the reactivity of the carbon surface (e.g. acidity, basicity). In order to develop a perspective on what further progress in the analysis of surface species and carbon surface reactivity using TPX might look like, a review of the state of the art is provided that focuses on identifying opportunities for the further advancement of TPX analysis. In this sense, temperature-programmed techniques will be subdivided into temperature-programmed desorption (TPD), temperature-programmed reduction (TPR), and temperature-programmed surface reaction (TPSR), with the focus on the analysis of sp^2 -hybridized carbons. Whenever possible, we try to discuss underlying chemical mechanisms and their implications for accurate TPX analysis, with an

emphasis on potential pitfalls and gaps of knowledge. Without intending to reiterate textbook knowledge extensively, the influence of the experimental setup and the impact of mass transfer limitations on TPX measurements are briefly discussed. Finally, a perspective on the future of temperature-programmed analysis techniques in carbon surface science is provided with the goal of stimulating the further development of this set of analytical methods.

2. GENERAL CONSIDERATIONS

In general, temperature-programmed techniques for the analysis of carbon surface species are carried out by subjecting the sample to a temperature ramp in either an inert or reactive atmosphere. This temperature ramp induces processes such as thermal decomposition, desorption, reduction, or catalytic transformations, which are detected by a suitable off-gas analysis as a function of temperature. Since every individual process is governed by intrinsic kinetic parameters that follow Arrhenius' law, the utilization of a temperature ramp allows them to be induced and detected in a time-separated manner. Accordingly, TPX analysis allows conclusions to be drawn about a wide range of different properties, such as the identity and quantity of physi- or chemisorbed species on the carbon surface, the strength of interaction between adsorbates and the carbon surface, or the reactivity of the carbon surface toward gaseous reactants (e.g., O_2 , CO_2 , H_2).

TPX analysis is generally subdivided according to the atmosphere that is used during the temperature ramp (Figure 2). In this context, temperature-programmed desorption (TPD) is generally carried out in inert atmospheres and is aimed at the analysis of adsorbates that are either present on the carbon surface before the experiment or are deliberately introduced as molecular probes (e.g., ammonia to characterize

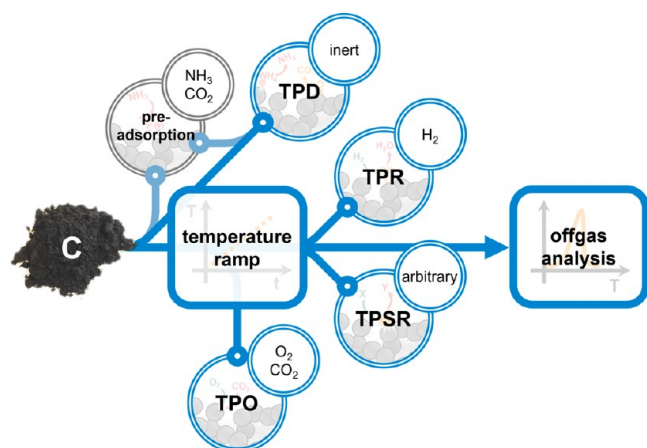


Figure 2. Temperature-programmed methods for carbon characterization make use of temperature ramps in order to initiate and detect heat-induced processes in a time-separated manner. Temperature-programmed desorption (TPD) is used to analyze adsorbed species (which might be deliberately introduced by a preadsorption step) in inert atmospheres. Temperature-programmed reduction (TPR) and temperature-programmed oxidation (TPO) probe the susceptibility for reduction and oxidation, respectively, and are carried out in the presence of hydrogen in the case of TPR and oxidants such as oxygen or carbon dioxide in the case of TPO. Temperature-programmed surface reactions (TPSRs) use the catalytic transformation of an arbitrary molecular probe in order to examine the reactivity of surface species in that particular catalytic process.

the surface acidity) by a preadsorption step before the temperature ramp is employed. The temperature ramp initiates the heat-induced desorption of adsorbates, thus offering information concerning the identity and quantity of adsorbates as well as the strength of interaction of adsorbates with the carbon surface, which correlates with the desorption temperature. Temperature-programmed reduction (TPR) is carried out in the presence of hydrogen (or other reducing species such as CO or CH₄) in order to examine the reduction of carbon surface species or even the carbon backbone. Similarly, temperature-programmed oxidation (TPO) uses temperature ramps in the presence of oxidants such as oxygen or carbon dioxide in order to probe the susceptibility of the carbon sample to oxidation. Finally, temperature-programmed surface reaction (TPSR) uses the catalytic transformation of an

arbitrary molecular probe in order to examine the reactivity of surface species in that particular catalytic process. Against this backdrop, this article is subdivided into three main chapters discussing temperature-programmed desorption, temperature-programmed reduction, and temperature-programmed surface reaction, with a focus on the characterization of carbon surface species in terms of identity, quantity, and reactivity. Temperature-programmed oxidation is not discussed, as it is not considered to be a method for carbon surface characterization and is thus not within the scope of this work.

Concerning the setup used to carry out temperature-programmed analysis of carbons, the online off-gas analysis and the reactor geometry demand particular attention. Online off-gas analysis for TPX experiments is required to offer an appropriate compromise between a high time resolution, low detection limits, and the ability to identify and quantify multiple species simultaneously. This compromise is best met by mass spectrometry or IR spectroscopy, since thermal conductivity detectors lack the ability to detect and quantify multiple species simultaneously and gas chromatography is not recommendable due to its low time resolution. At this point it should be noted that the terms “signal”, “peak”, and the like in the following refer exclusively to the outcomes of the actual TPX experiments and not to results (e.g., mass spectra and IR spectra) generated directly by the analytical system. As reactors, plug-flow setups and thermogravimetric balances are widely used. Plug-flow setups rely on a tubular reactor in which the carbon sample is fixed and the inert or reactive gas is passed directly through the sample bed. In the case of thermogravimetric balances, various reactor geometries combined with different flow regimes exist; however, mostly cup-shaped crucibles are used as sample holders, and the inert or reactive gas is rarely passed directly through the sample.^{12,13} The different flow regimes and reactor geometries of the two described setups lead to differences in the residence time distribution and the mass transfer behavior and in consequence to deviating analysis results. In case of TPD measurements in a thermogravimetric balance, a desorbing molecule leaving the pore system of a carbon sample must bridge the “zone of low convection” in the crucible above the sample by diffusion before being transported to the off-gas analysis by convection around the sample holder. In contrast, the gas flow directly through the sample bed in the plug-flow setup guarantees a

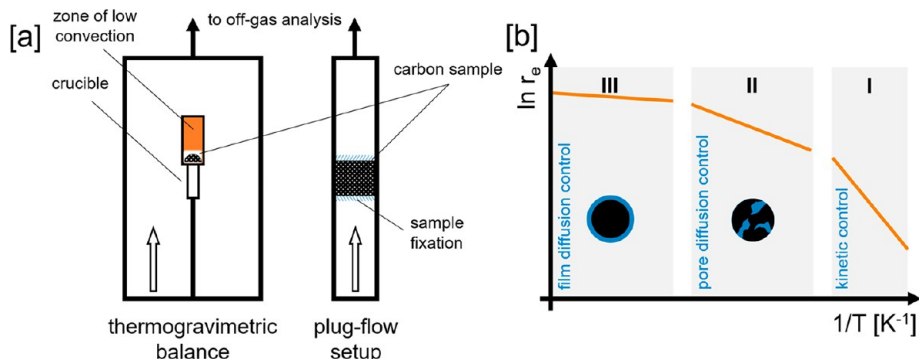


Figure 3. [a] Reactor geometry has a significant influence on mass transfer during TPX experiments. Zones of low convection in crucibles used in thermogravimetric balances represent a significant mass transfer barrier, especially in comparison with plug-flow setups. [b] The intrinsic reaction rate of a heterogeneous reaction taking place at the surface of a porous particle displays an exponential dependency on the temperature, while pore and film diffusion rates exhibit less pronounced temperature dependencies. In consequence, by applying heating ramps in TPX experiments, the effective reaction rate (r_e) may be governed by intrinsic kinetics (I), pore diffusion (II), and film diffusion regimes (III).

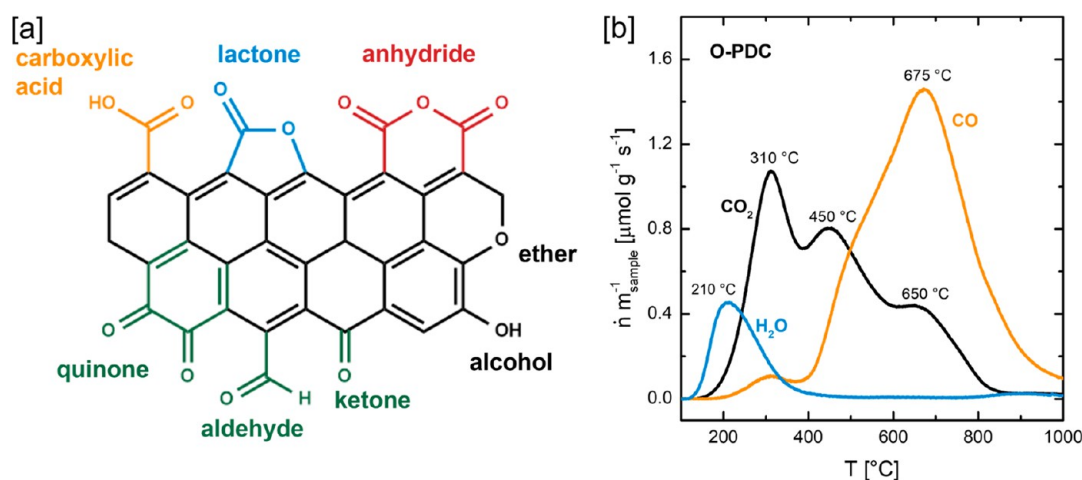


Figure 4. [a] Structures of various prominent surface oxides on carbon materials and [b] typical TPD desorption patterns of CO_2 , CO , and H_2O for a polymer-derived (phloroglucinol/formaldehyde) carbon oxidized with HNO_3 (heating rate of $5\text{ }^\circ\text{C min}^{-1}$, 30 mL min^{-1} He, 50 mg of sample, performed in a thermogravimetric balance). Reprinted with permission from ref 25. Copyright 2021 Elsevier.

much smaller offset between the desorption and detection of volatiles at the price of a lack of information on sample mass change provided by thermogravimetric balances (Figure 3).^{12,13}

The influence of mass transfer during TPX analysis of carbon materials is especially pronounced in case of experiments that rely on the interaction between a gaseous reactant and the carbon sample. Taking the temperature-programmed reduction of a carbon surface species in hydrogen as an example, the intrinsic reaction rate of reduction increases exponentially according to Arrhenius' law as the temperature increases. For the reaction to proceed, hydrogen has to be transported to the carbon surface, which is provided by a sequence of film diffusion and pore diffusion independent of the reactor setup, whereas the influence of temperature on the rate of diffusion is usually far less pronounced than on the intrinsic reaction rate.¹⁴ Consequently, as the temperature increases, the rate of hydrogen consumption exceeds the rate of hydrogen delivery, leading to a depletion of the hydrogen concentration at the carbon surface. In this situation, the observed reaction rate will be governed by the rate of hydrogen diffusion and as such will be limited by mass transfer. The extent to which the mass transfer limitation influences the result of the measurement and impedes the subsequent interpretation depends on experimental parameters (heating rate, gas flow rate, hydrogen concentration) as well as sample characteristics (particle size, porosity, catalytic impurities). Reactor geometry plays of course a pivotal role, as diffusion pathways tend to be significantly longer in sample holders commonly utilized in thermogravimetric balances compared to plug-flow setups in which reactive gases are passed directly through the sample bed. In this sense diagnostics are key, meaning that the presence or absence of internal or external diffusion limitations should be carefully checked, for example, by consulting the Weisz–Prater criterion and performing appropriate validation experiments (e.g., variation of flow rates, variation of heating rates).

The point to be emphasized is that the comparison of temperature-programmed experiments, especially those that rely on reactions of carbon with gaseous reactants, has to be treated with special caution. Experiments that are conducted in different setups, use different experimental parameters, or

examine samples of widely differing properties (e.g., porous versus nonporous, large versus small particles) can in principle only be compared on the basis of intrinsic kinetic parameters, while any mass transfer limitation must be excluded.

3. TEMPERATURE-PROGRAMMED DESORPTION

3.1. Characterization of Heteroatom Functional Groups. **3.1.1. Oxygen Functional Groups.** Due to the well-documented affinity of carbon materials for oxygen, most of the research effort with respect to temperature-programmed desorption has so far been directed toward the analysis of carbon surface oxides.^{7,15–21} Some commonly encountered oxygen surface groups are carboxylic acids and carboxylic acid derivatives such as lactones and carboxylic acid anhydrides. Furthermore, ethers, various alcohols, and carbonyl groups such as aldehydes, ketones, and quinones are common surface groups (Figure 4).^{16,22–24} Depending on their chemical structures, carbon surface oxides exhibit different thermal stabilities and decompose in a temperature range between 200 and 1200 $^\circ\text{C}$. In an inert atmosphere, typical decomposition products are CO_2 , which is released by the desorption of carboxylic acid derivatives, and CO , which is emitted during the thermal decomposition of alcohols, ethers, aldehydes, ketones, and quinones.¹⁶ As illustrated by Table 1, considerable effort has been directed toward assigning CO and CO_2 evolution maxima to individual surface oxides during TPD.

Most assignments are conducted by studying the reactivity of surface oxides and by combining various methods such as titration, XPS, and IR spectroscopy with TPD.^{18,19,27,35} In this context, one widely applied method of identifying the decomposition temperature of an individual surface oxide is the heat treatment of an oxidized carbon sample in inert atmosphere at a specified temperature and the subsequent analysis of the annealed sample by other analytical techniques.^{16,19,29,33,37} In addition, Barco and co-workers employed density functional theory (DFT) calculations using polyaromatic hydrocarbons as backbones to examine the thermal stabilities of various surface oxides.²⁸ Nevertheless, in some cases the assigned desorption maxima show considerable differences most likely caused by the structural diversity of the studied carbon materials (providing energetically different

Table 1. Desorption Temperatures and Decomposition Products of Various Prominent Carbon Surface Oxides

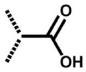
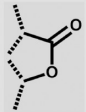
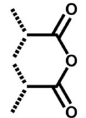
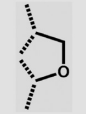
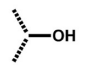
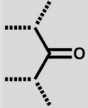
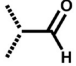
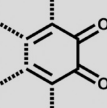
Surface oxide	Decomposition product(s)	Desorption temperature	Carbon material	Reference
Carboxylic acids 	CO ₂	327 °C	PDC ¹	[18]
		100 – 400 °C	PDC ¹	[20]
		327 °C	AC ²	[26]
		237 – 447	AC ³	[17]
		200 – 250 °C	Carbon fiber	[27]
		127 – 677 °C	PAH (DFT) ⁵	[28]
		340 °C	MWCNT	[29]
		310 °C	MWCNT	[30]
		300 °C	MWCNT	[31]
		252 °C	MWCNT	[32]
275 °C	MWCNT	[33]		
Lactones 	CO ₂	627 °C	PDC ¹	[19]
		627 – 727 °C	AC ³	[17]
		667 °C	AC ⁴	[16]
		350 – 400 °C	Carbon fiber	[27]
		190 – 650 °C	Graphite	[34]
		557 – 607 °C	PAH (DFT) ⁵	[28]
		650 °C	MWCNT	[29]
		625 °C	MWCNT	[30]
		750 °C	MWCNT	[31]
		252 – 620 °C	MWCNT	[32]
650 °C	MWCNT	[33]		
Anhydrides 	CO + CO ₂	627 °C	PDC ¹	[18]
		627 °C	PDC ¹	[19]
		547 °C	AC ⁴	[16]
		527 – 627 °C	AC ³	[17]
		777 °C	AC ²	[26]
		> 300 °C	AC ⁶	[35]
		350 – 450 °C	Carbon fiber	[27]
		357 – 527 °C	PAH (DFT) ⁵	[28]
		470 °C	MWCNT	[29]
		440 °C	MWCNT	[30]
		470 °C	MWCNT	[31]
		315 – 620 °C	MWCNT	[32]
		435 – 460 °C	MWCNT	[33]
Ethers 	CO	700 °C	PDC ¹	[20]
		> 670 °C	MWCNT	[29]
		960 °C	MWCNT	[31]
		620 – 800 °C	MWCNT	[32]
		735 °C	MWCNT	[33]
Alcohols 	CO	410 – 510 °C	PDC ⁷	[36]
		667 – 717 °C	AC ³	[17]
		632 °C	AC ⁴	[16]
		600 – 700 °C	Carbon fiber	[27]
		700 °C	MWCNT	[29]
		725 °C	MWCNT	[31]
		620 – 800 °C	MWCNT	[32]
735 °C	MWCNT	[33]		

Table 1. continued

Surface oxide	Decomposition product(s)	Desorption temperature	Carbon material	Reference
Ketones 	CO	700 °C	PDC ¹	[20]
		680 °C	PDC ⁷	[36]
		800 – 900 °C	Carbon fiber	[27]
		387 & 1367 °C	PAH (DFT) ⁵	[28]
		280 °C	MWCNT	[29]
		725 °C	MWCNT	[31]
		800 – 1000 °C	MWCNT	[32]
920 °C	MWCNT	[33]		
Aldehydes 	CO	700 °C	PDC ¹	[20]
		680 °C	PDC ⁷	[36]
		800 – 900 °C	Carbon fiber	[27]
		847 – 882 °C	PAH (DFT) ⁵	[28]
		280 °C	MWCNT	[29]
		310 °C	MWCNT	[30]
		500 °C	MWCNT	[31]
800 – 1000 °C	MWCNT	[32]		
Quinones 	CO	700 °C	PDC ¹	[20]
		877 °C	AC ²	[26]
		817 – 877 °C	AC ³	[17]
		807 °C	AC ⁴	[16]
		800 – 900 °C	carbon fiber	[27]
		700 °C	MWCNT	[29]
		> 670 °C	MWCNT	[30]
		800 – 1000 °C	MWCNT	[32]
		920 °C	MWCNT	[33]

¹Polymer-derived carbon; micro- and mesoporous carbon derived from a phenol/formaldehyde resin. ²Activated carbon produced by the pyrolysis of olive stones and steam activation. ³Activated carbon produced by the pyrolysis of coconut shell and steam activation. ⁴NORIT ROX 0.8 activated carbon. ⁵DFT study using poly aromatic hydrocarbons (PAH) as a backbone for examining the thermal stability of various functional groups. ⁶Activated carbon produced by the pyrolysis of almond shells and steam activation. ⁷Polymer-derived carbon; amorphous micro- and mesoporous carbon derived from a soft-template approach involving phloroglucinol/formaldehyde as carbon source and Pluronic F127 as soft-template.

chemisorption sites) and by the chemical similarity of carbon surface oxides, meaning that even the combination of numerous analytical methods sometimes fails to provide unambiguous results. In light of this situation, selectively functionalized reference materials were recently proposed by Herold et al. as a feasible approach to address this challenge (Figure 5).³⁶ For instance, a reference material for hydroxyl groups could be synthesized by the reduction of a preoxidized polymer-derived carbon with lithium aluminum hydride, which allowed the direct determination of the desorption maxima of primary alcohols (410 °C) and phenolic hydroxyl groups (510 °C). However, it should be noted that in case of a quantitative reduction of the oxygen surface ensemble, no CO₂ evolution would be expected. Thus, the observed CO₂ evolution is either a sign of an incomplete reduction or the reoxidation of the carbon surface as a result of air exposure after the LiAlH₄ treatment, indicating that this organic chemistry approach toward reference materials may be feasible but still requires improvement.

However, not all functionalization strategies are feasible for synthesizing reference materials for TPD, as widely deployed functionalization strategies for carbon materials involving the attachment of specific functional groups via linkers to the carbon surface^{38,39} were proven to be inadequate for producing

reference materials for TPD. Since the thermal stability of grafted moieties tends to be limited by the stability of the corresponding linker, desorption temperatures of linker-bound functionalities differed significantly from those of (cyclic, conjugated) surface oxides introduced by the oxidation of the carbon matrix, which are situated directly on the carbon surface.³⁶ In this sense, besides LiAlH₄ reduction, the enrichment of carbon surfaces with specific surface oxides in direct contact with the carbon matrix could also be demonstrated by combining selective desorption by heat treatment with hydrolysis and condensation of functional groups introduced in advance by oxidation.²⁵ However, even though heat treatments are widely applied for the production of carbons with different surface oxide profiles, the selectivity is often poor due to overlapping desorption ranges of individual surface oxides. Viable routes to useful analytical standards therefore appear to be leading either via direct selective chemical transformation (using methods of organic chemistry) of surface oxides that are already present or via selective oxidations that allow the targeted introduction of individual surface oxides.

In TPD patterns of nonselectively oxidized carbon materials, the number of CO and CO₂ evolution maxima typically falls short of the number of individual oxygen groups expected on

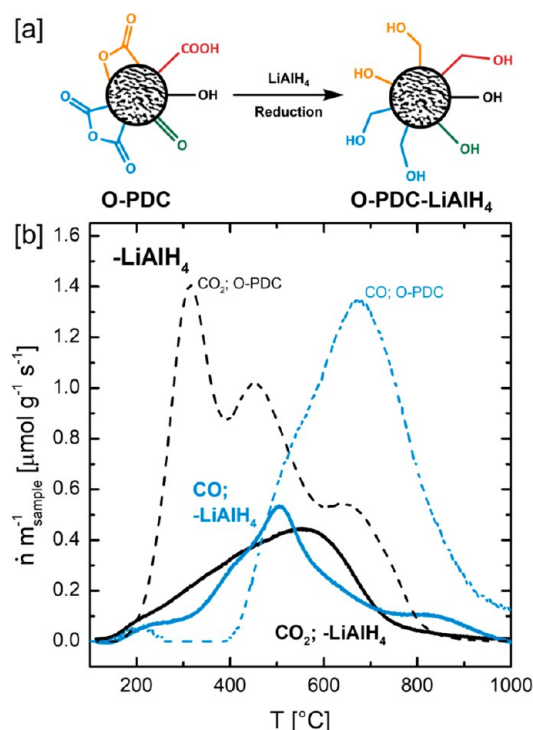


Figure 5. [a] The direct reduction of a HNO₃-oxidized polymer-derived carbon (O-PDC) with LiAlH₄ yields a carbon surface that is occupied solely by hydroxyl groups, thus representing a reference material for hydroxyl groups. [b] Comparison of the TPD CO and CO₂ emission profiles of the oxidized carbon (O-PDC, dashed lines) and the LiAlH₄-reduced carbon (O-PDC-LiAlH₄, solid lines; heating rate of 5 °C min⁻¹, 30 mL min⁻¹ He, 50 mg of sample, performed in a thermogravimetric balance). Reprinted with permission from ref 36. Copyright 2021 Elsevier.

the corresponding material. The reason for this is found in the considerable signal width, where the overlap of the broad desorption peaks of individual surface oxides results in the observed shape of the CO and CO₂ evolution profiles. Signal broadening is often attributed to oxygen chemisorption at sites that differ energetically, whereas a broad distribution of various chemisorption sites is expected, especially for disordered sp³/sp²-hybridized carbon.^{16,35} On the other hand, the signal width

is heavily influenced by nonintrinsic factors such as experimental parameters (heating rate, volume flow of inert gas), the residence time behavior of the employed apparatus, mass transport limitations caused by pore diffusion, etc. In order to circumvent this signal overlap and gain quantitative information, Figueiredo, Pereira, and co-workers proposed the deconvolution of the CO and CO₂ evolution profiles, whereas the desorption signal of every expected surface oxide is modeled with a Gaussian profile (Figure 6).^{16,17} Gaussian functions are utilized under the assumption that every surface oxide exhibits a random distribution of binding energies, thus requiring symmetrical model functions. Starting parameters for the fit are usually desorption maxima of expected surface oxides, while the temperature range for the width of the model functions is also often restricted to a reasonable interval that is similar for all modeled surface groups. Finally, secondary reactions are assumed to be negligible.¹⁷

Since this deconvolution technique appeals by simplicity and opens a pathway for the quantification of TPD results, a wide variety of studies have applied this method for the analysis of carbon surface oxides.^{15–17,25,36,40–45} Comparing TPD quantification results to those of titration methods and XPS experiments enables a valuable “sanity check” of the overall analysis of carbon surface oxide ensembles and helps to eliminate ambiguities.^{15,25,36,46,47}

Beyond mathematical fitting, Dungen et al. recently proposed a method that relies on nonlinear temperature profiles to disentangle the overlapping desorption range of different surface oxides (Figure 7).⁵² In this context, heating ramps are interrupted by isothermal segments whose temperature is chosen in a manner that it lies slightly above the decomposition temperature of a given surface oxide. Hence, the temperature is raised above the desorption maximum of this surface oxide by a heating ramp, while the subsequent isothermal step allows the complete decomposition of this surface oxide without interference from the desorption of the surface oxide exhibiting the next-highest thermal stability. Accordingly, this method heavily relies on the correct choice of the temperature of the isothermal steps, which are selected such that the observed CO and CO₂ evolution peaks exhibit symmetrical shapes, indicating that only one surface oxide undergoes decomposition. Thus, an optimized temperature profile was developed using multiwalled carbon nanotubes as a

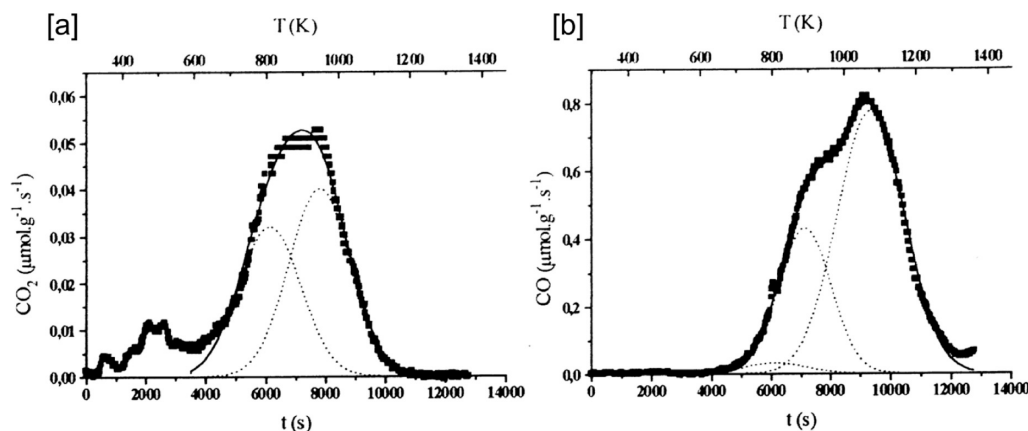


Figure 6. Deconvolution of the [a] CO₂ and [b] CO desorption profiles using sets of Gaussian functions. TPD of NORIT ROX 0.8 activated carbon oxidized with 5% O₂ at 425 °C (heating rate of 5 °C min⁻¹, 23.5 mL min⁻¹ He, 100 mg of sample, performed in a tubular reactor). Reprinted with permission from ref 16. Copyright 1999 Elsevier.

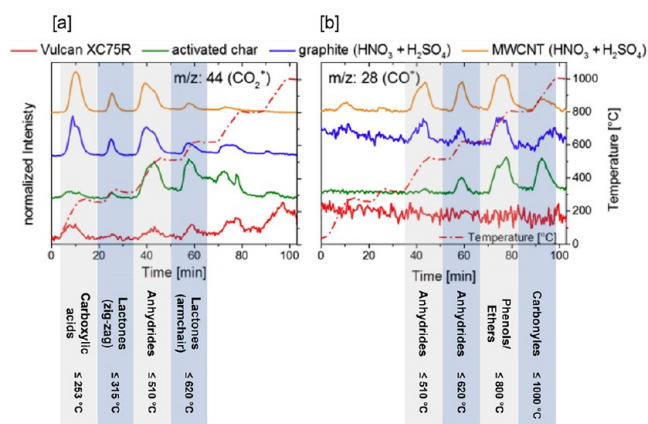


Figure 7. Nonlinear temperature-programmed desorption enables the disentanglement of overlapping desorption ranges. Isothermal segments positioned slightly above the decomposition temperature of a specific surface oxide allow its complete desorption without interference from the decomposition of surface oxides exhibiting higher thermal stabilities. [a] CO_2 and [b] CO emission profiles from the nonlinear TPD analysis of a carbon black (Vulcan XC75R), an activated char, oxidized graphite, and oxidized MWCNTs (heating rate of $20\text{ }^\circ\text{C min}^{-1}$ and 70 mL min^{-1} Ar, performed in an thermogravimetric balance). Adapted from ref 32 under a CC-BY-4.0 license (<https://creativecommons.org/licenses/by/4.0/>); annotations were added to the original.

model material, which demonstrated the feasibility of the proposed method.³² Using the same temperature profile, graphite, an activated char, and carbon black were also analyzed, showing that the specified temperature program was well-suited for the separation of surface oxide desorption signals in graphitic materials (MWCNTs, graphite) (Figure 7). However, the analysis of the activated char in particular showed that CO_2 emitting groups could not be separated as well compared to the graphitic materials. Many reasons for this finding are conceivable, such as misplaced isothermal steps, broader desorption temperature ranges due to pore diffusion limitations, a broader distribution of adsorption energies as a consequence of the disordered carbon backbone, and so on. However, once baseline-separated, the CO and CO_2 emission of individual surface oxides can be easily quantified by signal integration. Analogous to the mathematical fitting procedure,

to obtain reliable quantification results, one must ensure that side reactions can be neglected.³²

Ishii et al. took a different path to discriminate surface oxides with overlapping desorption ranges. Their approach involved the isotopic labeling of specific surface oxides via the exchange of acidic protons bound to carboxylic acid groups and phenols with deuterium by treating an oxidized carbon sample with D_2O .⁴⁸ While the desorption range of carboxylic acids is well-known, the decomposition of phenols coincides with that of ethers. Since both surface oxides emit CO upon decomposition, the unambiguous quantification of phenols and ethers has been very challenging. Employing the isotopic labeling approach, the decomposition of deuterium-labeled hydroxyl groups yields D-terminated edge sites, which emit D_2 or DH when the temperature exceeds $1000\text{ }^\circ\text{C}$ (Figure 8). Under the assumption that abundant H-terminated edge sites are nonprotic and are consequently not affected by the D_2O treatment, the number of phenol groups can be accurately determined by deconvoluting the CO_2 and CO emission profiles and subsequently taking the high-temperature emission of D_2 and DH into account. It should be noted, however, that the interpretation of the emission profiles of isotope-labeled species represents a challenge, as several side reactions involving isotope exchange between gas-phase and surface species are possible due to the porous structure of the activated carbon.⁴⁸

3.1.2. Side Reactions of Oxygen Surface Group Analysis.

Considering the chemical compounds involved and temperatures applied, there are several possible side reactions, including the readsorption of volatile carbon oxides on active sites on the carbon surface to form another type of surface oxide. In this context, the surface oxides yielded upon readsorption may undergo decomposition in a different temperature range compared to the initial surface species and, following the Boudouard equilibrium, might additionally emit CO_x species upon decomposition that are different from the adsorbed CO_x species. (Figure 9). In either case, the TPD emission profile is altered, since either the decomposition product emission is detected at a temperature that does not coincide with the desorption temperature of the original surface species or the true decomposition product cannot be detected due to interconversion between CO and CO_2 . The latter process can be excluded by performing TPD experiments

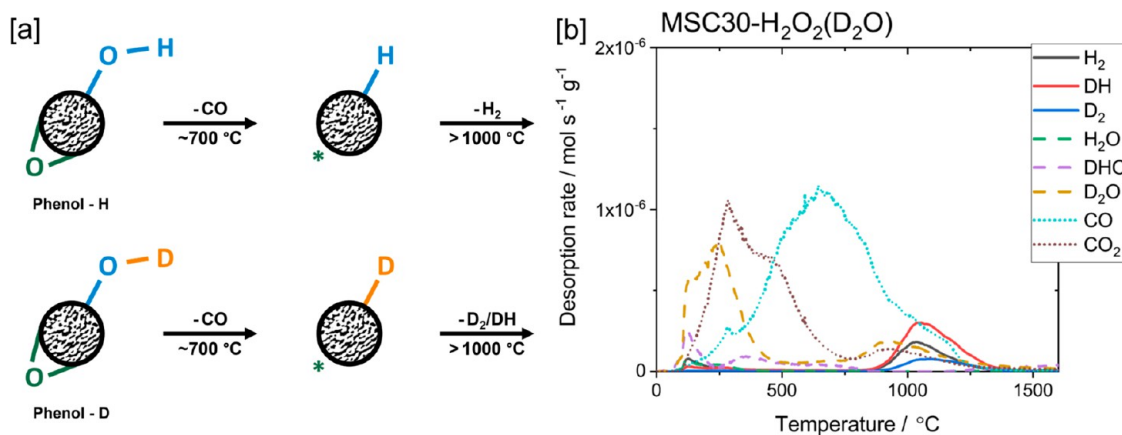


Figure 8. [a] Deuterium labeling of acidic groups such as phenols enables their discrimination from surface groups with similar decomposition temperature such as ethers. [b] High-temperature TPD of H_2O_2 -oxidized activated carbon, which was deuterium-labeled by proton exchange in D_2O (heating rate of $10\text{ }^\circ\text{C min}^{-1}$ at $1 \times 10^{-5}\text{ Pa}$). Reproduced with permission from ref 48. Copyright 2020 Elsevier.

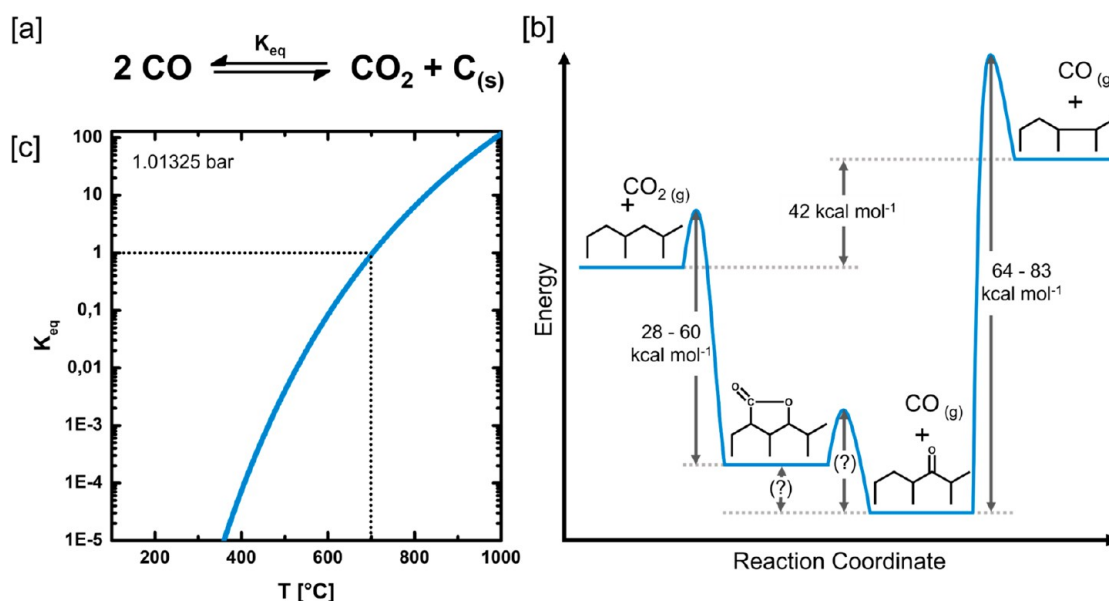


Figure 9. [a] Boudouard equilibrium. [b] Model of CO and CO₂ interconversion using lactone and carbonyl surface intermediates. Reproduced with permission from ref 50. Copyright 1988 American Chemical Society. [c] Temperature dependency of the equilibrium constant of the Boudouard reaction.

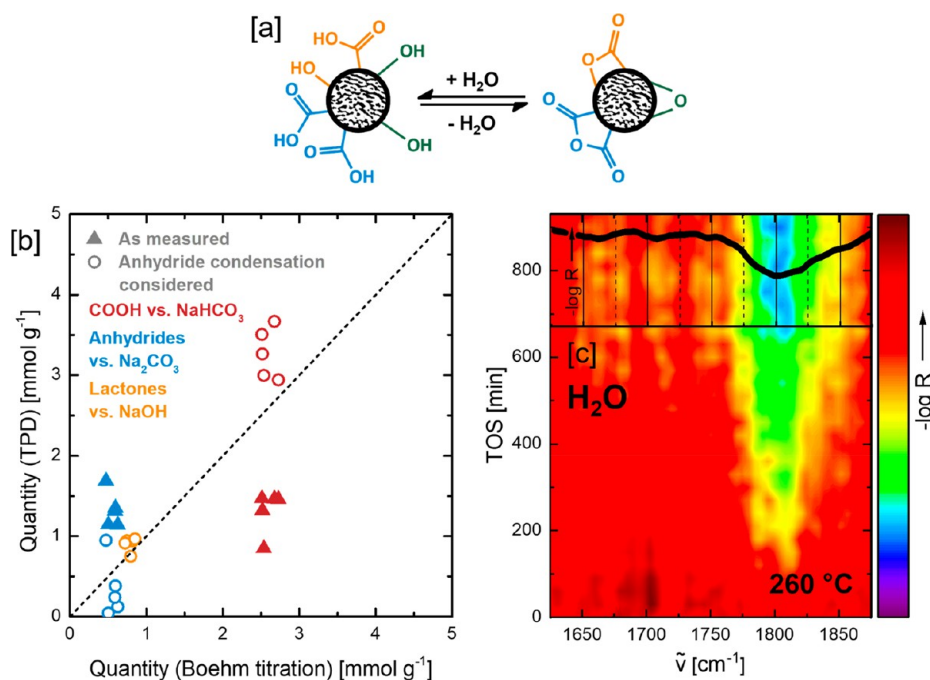


Figure 10. [a] Schematic illustration of possible condensation and hydrolysis reactions of carbon surface oxides. [b] Correlation of the results of Boehm titration (consumption of NaHCO₃, Na₂CO₃, and NaOH) with quantification results (COOH, anhydrides, and lactones) obtained by fitting the TPD CO₂ emission profile. Full symbols display the quantification results “as measured”, while the empty symbols display the quantification results under consideration of the condensation of carboxylic acids to anhydrides, which is indicated by the emission of H₂O during TPD. Reprinted with permission from ref 25. Copyright 2021 Elsevier. [c] In situ DRIFT spectrum of an oxidized polymer derived carbon at 260 °C in an atmosphere of 1.5 vol % H₂O in He. The IR spectrum between 1625 and 1875 cm⁻¹ (carbonyl region) after 900 min on stream is depicted in the upper part of the graphic. The loss of absorption over 900 min time on stream can be attributed to the decreasing concentration of carboxylic anhydrides (absorption maxima of carboxylic anhydrides were determined to be located at 1792 and 1852 cm⁻¹). Reproduced from ref 45 under a CC-BY-4.0 license (<https://creativecommons.org/licenses/by/4.0/>); the arrangement of the original was modified.

at different heating rates while measuring the ratio of CO and CO₂ emission. However, instead of the ratio of the total amount of emitted CO and CO₂ being constant, which is expected in the absence of this interconversion, it is often found that the CO/CO₂ ratio is indeed dependent on the

heating rate due to the kinetics of interconversion.^{32,49} The Boudouard equilibrium is closely connected to the readorption of CO and CO₂ earlier mentioned, since there is broad evidence that both reactions (the conversion of CO₂ and solid C to CO and vice versa) proceed via surface oxides as

intermediates.⁵⁰ The adsorption of CO and CO₂ was extensively studied by Hall et al. and Marchon et al., who performed similar experiments on coal chars and polycrystalline graphite, respectively.^{34,49,50} In either case, the carbon material was “degassed” in an inert atmosphere at temperatures exceeding 1000 °C (and remained in an inert atmosphere) before introducing CO or CO₂ at various temperatures and subsequently performing TPD experiments. Since the carbon materials were only exposed to inert atmospheres (He or ultrahigh vacuum) after thermal degassing, reactive sites created by desorption of volatile species remained unsaturated, and enabled chemisorption of significant amounts of CO and CO₂. Independent of the chosen adsorbate, subsequent TPD produced both CO and CO₂, providing evidence for the interconversion of CO and CO₂. Even after chemisorption of CO₂, CO was the main desorption product detected during TPD, whereas multiple emission maxima were observed over a broad temperature range.^{34,49,50} In this context, the identity of the species formed by CO or CO₂ chemisorption (or the occupied chemisorption site) appeared to be highly dependent on the temperature at which the adsorption experiment was performed.⁵⁰ Isotope labeling experiments further highlighted the complexity of the system, as the chemisorption of a mixture of C¹⁶O₂ and C¹⁸O₂ produced a significant amount of C¹⁶O¹⁸O in the subsequent TPD experiment.⁵⁰

Hall and co-workers additionally studied the influence of impurities and the specific surface area of the carbon material on the shifting ratio of the total amount of emitted CO and CO₂ when the heating rate was varied. By comparing demineralized and pristine coal chars, they reached the conclusion that impurities played a minor role, since the demineralized char showed the most severe dependence of the CO/CO₂ ratio on the heating rate of all samples examined. In contrast, the specific surface area did have a pronounced influence, as the interconversion of CO and CO₂ was only observed with porous chars, whereas nonporous coal chars (2 m² g⁻¹ specific surface area) did not show any shift in the CO/CO₂ ratio upon variation of the heating rate.⁴⁹ It should be noted that while the thermodynamics of the Boudouard equilibrium are well-known, this experiment clearly implies that the extent to which CO/CO₂ interconversion influences TPD experiments is governed by the corresponding kinetics and thus is heavily dependent on sample characteristics such as pore and particle size distribution and the reactor geometry, thus limiting the comparability of results from different carbon samples and TPX setups.

Besides CO₂ and CO, the evolution of chemisorbed H₂O is often detected during TPD analysis and has been suggested by several groups as an indicator of condensation reactions between neighboring functional groups (Figure 4).^{18,25,26,29,31,37,46,51} In this sense, carboxylic acid groups in spatial proximity can form carboxylic anhydrides, carboxylic acids and hydroxyl groups can form lactones, while the condensation of neighboring hydroxyl groups yields ethers (Figure 10).^{26,29} Condensation reactions, as indicated by the emission of chemisorbed H₂O, lead to a shift in the apparent surface concentration of acidic groups, namely the conversion of strongly acidic carboxylic acid groups to anhydrides and lactones, which exhibit higher pK_a values. In consequence, the influence of condensation reactions can be studied by comparing titration techniques with quantitative TPD experiments.^{15,23,47} In case of Boehm titration, a carbon material is neutralized by prolonged contact to bases of different pK_i

(NaHCO₃, Na₂CO₃, and NaOH); the weak base selectively deprotonates strong carboxylic acids, the medium-strength base Na₂CO₃ neutralizes carboxylic acids and anhydrides, while NaOH as a strong base additionally hydrolyses lactones and deprotonates phenolic OH groups. If the shift in the concentration of CO₂-emitting surface oxides due to condensation reactions is ignored, the comparison of TPD quantification and the consumption of the corresponding bases during Boehm titration yields a rather poor correlation. In particular, the concentration of carboxylic acids, main reactants in condensation reactions, is significantly underestimated by TPD. However, under the assumption that the observed water is exclusively produced by the reaction of carboxylic acids to form anhydrides, the amount of emitted water can be used to recalculate the surface concentration of carboxylic acids and anhydrides, which subsequently correlates much better to the results of Boehm titration (Figure 10).²⁵

Nevertheless, it has to be noted that this approach neglects the formation of lactones and ethers as sources of water emission, which consequently leads to an overestimation of the carboxylic acid content in combination with an underestimation of the carboxylic anhydride concentration. In the case of high surface oxide coverages (20 at. %), condensation reactions have even deliberately been used in order to manipulate the carbon surface oxide ensemble.²⁵ In the presence of water vapor, the hydrolysis of carboxylic anhydrides, lactones, and ethers is conceivable. In this context, the hydrolysis of anhydrides could be proven by studying an oxidized carbon exposed to a stream of 1.5 vol % water in N₂ at 260 °C with in situ diffuse reflectance infrared Fourier transform spectroscopy (DRIFTS, Figure 10c).^{45,52}

3.1.3. Nitrogen Functional Groups. One of the most distinctive features of N-doped carbon, especially in comparison with oxygen, is the presence of bulk N species in addition to surface N species. The bulk doping of N is facilitated by the electronic structure of N as well as its similar atomic size compared to C (atomic radii 190 pm for C and 179 pm for N) and the similar length of the C–N (141 pm) and C=C (142 pm) bonds.^{53,54} Bulk N is represented by quaternary N species that substitute a C atom in the graphite lattice plane, forming three bonds to neighboring C atoms. The lone electron pair contributes to the π -system, resulting in a positively charged N atom. All other N species frequently discussed are located at the surface or edges of the carbon material and are represented by amino groups, imines, and nitriles in addition to pyridine and pyrrole moieties in total absence of oxygen. However, since oxygen contamination (e.g., by air exposure, moisture, and carbon precursors) can scarcely be excluded, mixed-atom species such as nitro groups, nitrite esters, amides, lactames, and imides are usually also present on N-doped carbon (Figure 11).

Even though TPD analysis of N-doped carbon materials has been executed in various studies, the technique is, especially in comparison to the TPD analysis of surface oxides, less mature.^{55,56,59,62–64} As illustrated in Table 2, the inert-atmosphere decomposition temperatures reported in the literature do not necessarily coincide, and there is some divergence concerning the decomposition products of individual N species. However, using a combination of TPD and XPS, most studies reach the general conclusion that the thermal stability of N species follows the sequence quaternary N > pyridinic N > pyrrolic N > nitrile N > nitro N and amino N.^{33,60,65,66} In this context, it has to be noted that conjugated

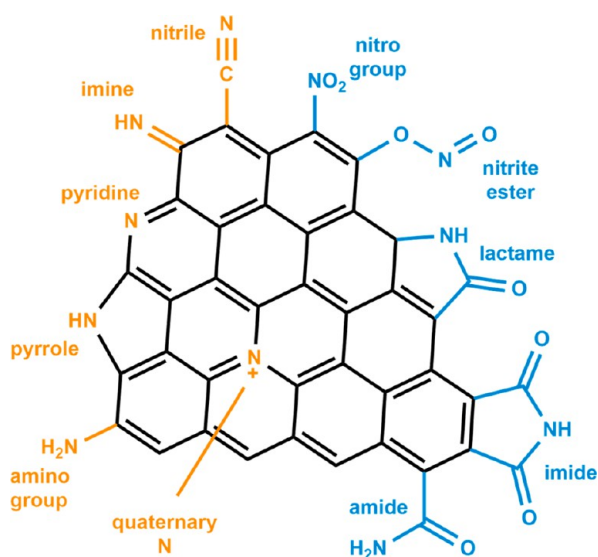


Figure 11. Structures of various prominent N species (orange) and mixed N/O species (blue) present on N-doped carbon.

N species such as quaternary N and pyridinic N in particular exhibit very high decomposition temperatures. In the case of quaternary N, Fujisawa et al. managed to detect significant amounts in MWCNTs annealed at temperatures up to 1500 °C, indicating that the thermal stability of some N species surpasses the temperature range accessible to common TPD setups.⁶¹ The most frequently observed decomposition products of N species are hydrogen cyanide (HCN), ammonia (NH₃), and dinitrogen (N₂); in the presence of surface oxides, nitric oxide (NO) and isocyanic acid (HNCO) are also emitted upon thermal desorption. Consequently, exposure to oxygen complicates the straightforward TPD analysis of N species on carbon, as the number of potential decomposition mechanisms and the possibility for side reactions increase, which is reflected by the literature reports of more than one (N-containing) decomposition product per functional group (Table 2). Analogous to the discussion in the context of the TPD analysis of carbon surface oxides, desorption signals of individual N species often exhibit a significant width, which may be caused by energetically differing chemisorption sites, mass transfer limitations, the geometry of the experimental setup, and the experimental parameters. In order to address the resulting overlap of the desorption signals, the deconvolution of TPD emission profiles was carried out by Arkhipova et al., who adopted a model based on “bi-Gaussian” curves that allowed them to also account for signals of asymmetric shape.⁵⁷

It should be noted that the interpretation of the TPD emission profiles of N-doped carbon is complicated to a considerable extent by thermally induced side reactions in which N-species are transformed by dehydration, condensation, decarbonylation, and rearrangement reactions (Figure 12). In this context, Stańczyk et al. used precursors with specific N-functional groups such as amino groups, nitriles, and pyridinic N (mostly derivatives of anthracene) and studied the chars obtained by the pyrolysis of these precursors at temperatures between 460 and 800 °C using XPS.⁶⁵ As expected, the authors found that functional groups that participated in aromatic structures exhibited a significantly higher temperature tolerance compared to functional groups

simply attached to an aromatic backbone. However, cyclic conjugated N species showed a high tendency to mutually convert into each other, as illustrated by the example of the low-temperature (460 °C) carbonization of a precursor containing exclusively pyridinic N; pyrrolic N was found to account to up to 50% of the N species of the resulting char. Highlighting these interconversions, it was found that regardless of the functionalization of the precursor, the ensembles of N species in chars obtained by high-temperature pyrolysis (800 °C) exhibited nearly identical compositions, with pyridinic, pyrrolic, and quaternary N accounting each for ca. 1/3 of the detected N-species.⁶⁵ Generally, thermolabile functional groups tend to be converted in multiple steps to cyclic species conjugated with the carbon matrix, which exhibit a significantly higher temperature resistance compared to the initial species.^{33,58,60} In this manner, amino groups may condense with an adjacent carboxylic acid group to form a lactame, which may be converted to a pyrrole species by the loss of CO. This pyrrole species in turn may be subsequently transformed via rearrangement reactions to pyridinic or highly temperature-stable quaternary N species.^{33,58,59,67,68} As a result, the detection of the decomposition of a particular functional group is often the consequence of a cascade of previous transformations, rendering the deduction of the original species a major challenge (Figure 12).

Another nontrivial phenomenon is the observation that N-doped carbons often emit considerable amounts of N₂. The formation of this decomposition product requires an interaction between two N species, and a number of studies come to the conclusion that some form of surface mobility of N functionalities exists.^{33,60} However, besides the interaction of two N functional groups on the carbon surface, the reaction of N-containing gaseous decomposition products with chemisorbed N-species is also conceivable.⁶³ Considering the thermal instability of nitro groups, the observation of NO emission at high temperatures also indicates the occurrence of interactions between neighboring species or the reaction of decomposition products with surface functional groups (Figure 13).^{57,64,69}

3.1.4. Sulfur Functional Groups. Another type of heteroatom species on carbon surfaces that can be probed via TPD is sulfur. Induced by increasing temperatures, S species on carbon develop volatiles such as sulfur dioxide (SO₂), carbonyl sulfide (SCO), carbon disulfide (CS₂), and hydrogen sulfide (H₂S).^{70–76} Sulfur predominantly forms surface groups on carbon but is also able to participate in conjugated systems by means of its lone electron pairs.⁵³ It should be noted that the C–S bond is much longer (171 pm in thiophene) than the C=C bond in aromatic systems (142 pm) while the atomic radius of S (214 pm) is larger compared to that of C (190 pm), which consequently leads to to nonplanar, distorted structures in S-doped carbons.^{54,77,78} Owing to the challenges of oxygen exclusion and the popularity of S-doping methods involving H₂SO₄, mixed-atom functional groups usually occur on S-doped carbon in various forms and states of oxidation (Figure 14).^{79,80} Mixed oxygen/sulfur functional groups are typically represented by species such as sulfonic acids, sulfones, sulfoxides and thioesters, while sulfur in a lower state of oxidation is present in form of thiols, sulfides, and thiophene-like functional groups.

In general, literature reports on the desorption temperature ranges (obtained by combination of XPS, FTIR, and TPD) for mixed oxygen/sulfur functional groups tend to coincide, while

Table 2. Decomposition Products and Desorption Temperature of Various Prominent N-Species and Mixed N/O Species on Carbon during Temperature-Programmed Desorption

Nitrogen species		Decomposition product(s)	Desorption temperature	Carbon material	Reference
Amino groups		NH ₂ , NH ₃	800 °C	Carbon fiber ¹	[55]
Nitro groups		NO	407 °C	AC ²	[56]
		NO (nitrite esters)	300 °C	MWCNT ³	[57]
		NO (nitro groups)	400 °C	MWCNT ³	[57]
Nitriles		CN	700 – 1000 °C	Carbon fiber ¹	[55]
		HCN	250 °C	MWCNT ⁴	[33]
Imines		HCN	700 – 1000 °C	Carbon fiber ¹	[55]
Amides		HCN	650 °C	AC ⁵	[58]
		CO, NH ₃ , HCN	700 °C	AC ⁶	[59]
Imides		CO ₂ , HCN, HNCO	500 °C	MWCNT ⁴	[33]
		HCN	950 °C	AC ⁵	[58]
Lactams		NH ₂ , NH ₃	800 °C	Carbon fiber ¹	[55]
		CO, HCN, HNCO	680 °C	MWCNT ⁴	[33]
		HCN	950 °C	AC ⁵	[58]
		CO, NH ₃ , HCN	700 °C	AC ⁶	[59]
Pyrroles		HCN, HNCO	600 – 1100 °C	MWCNT ³	[57]
		HCN, H ₂	785 °C	MWCNT ⁴	[33]
		NH ₃	827 °C	PDC ⁷	[60]
Pyridines		N, CN	960 °C	Carbon fiber ¹	[55]
		HCN, HNCO	600 – 1100 °C	MWCNT ³	[57]
		HCN, H ₂	905 °C	MWCNT ⁴	[33]
		HCN	950 °C	AC ⁵	[58]
Pyridine N-oxides		NO, N ₂	223 – 423 °C	PDC ⁷	[60]
Quaternary N		HCN, HNCO	1050 °C	MWCNT ³	[57]
		-	>1500 °C	MWCNT ⁸	[61]

¹Carbon fiber derived from a phenol/formaldehyde fiber activated with steam or carbon dioxide and N-doped via ammonia treatment at various temperatures. ²Activated carbon oxidized with HNO₃ at 80 °C. ³MWCNTs grown with acetonitrile as the C and N source and oxidized with HNO₃. ⁴MWCNTs doped by HNO₃ oxidation prior to an ammonia treatment in a temperature range between 300 and 700 °C. ⁵Norit activated carbons subjected to HNO₃ oxidation prior to ammonia treatment at 200 °C. ⁶Norit activated carbon treated with ammonia at various temperatures. ⁷Polyacrylonitrile-derived carbon. ⁸MWCNTs synthesized by the pyrolysis of mixtures of ferrocene and benzylamine.

the assignment of decomposition temperatures for aliphatic and aromatic sulfides shows some ambiguity.⁸² However, most reports reach the conclusion that the thermal stability of sulfur species on carbon more or less follows the sequence aromatic sulfides > aliphatic sulfides > thioesters > sulfoxides and sulfones > thiols and sulfonic acids (Table 3).^{73,82,89} Analogous to the investigation of O and N species on carbon, several studies carried out a deconvolution of the TPD emission profiles of typical decomposition products of sulfur species such as SO₂.^{82,87,88} Some sulfur functional groups appear to

exhibit a very high thermal stability, as proven by the observation of considerable sulfur residues in samples of S-doped carbon after TPD experiments that reached peak temperatures of 1200 °C.⁷³ These high-temperature stable sulfur species are commonly assigned to be thiophenic sulfides.⁷³ Oxidized decomposition products of sulfur functional groups such as SO₂ or SCO are assigned to every sulfur species present on carbon materials, regardless of the state of oxidation. In the case of thiols or sulfides, this assignment is justified by the presence of chemisorbed oxygen on the studied

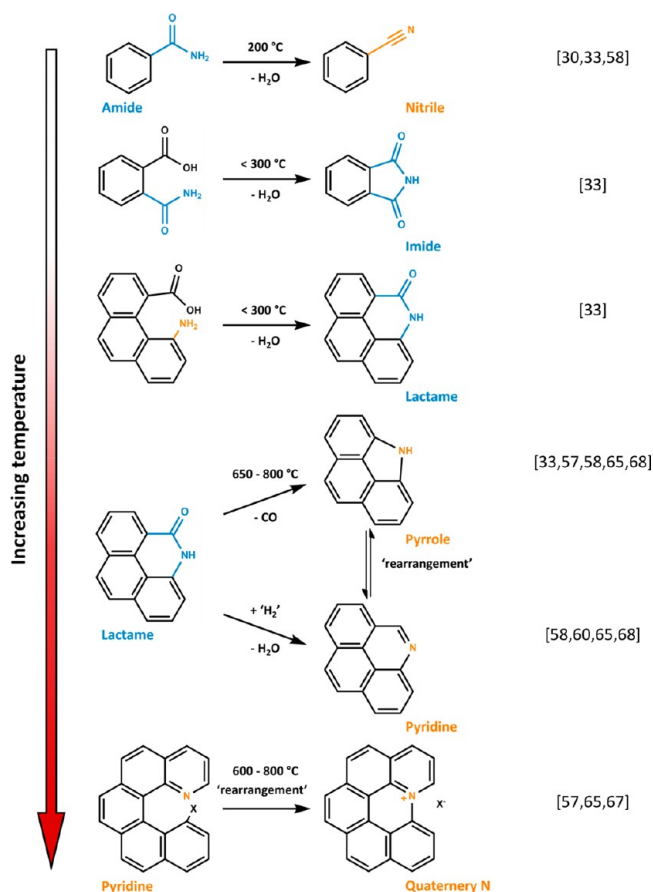


Figure 12. Possible temperature-induced structural evolution of N-species during the TPD analysis of N-doped carbon.

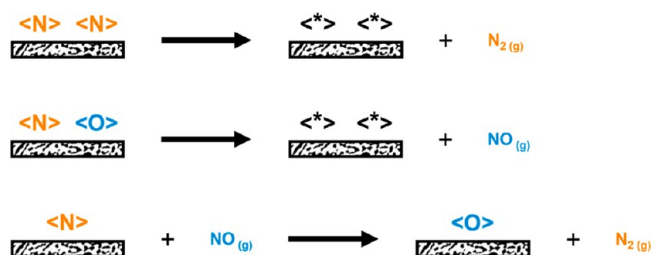


Figure 13. Possible side reactions during the TPD analysis of N-doped carbon that produce N_2 and high-temperature NO .

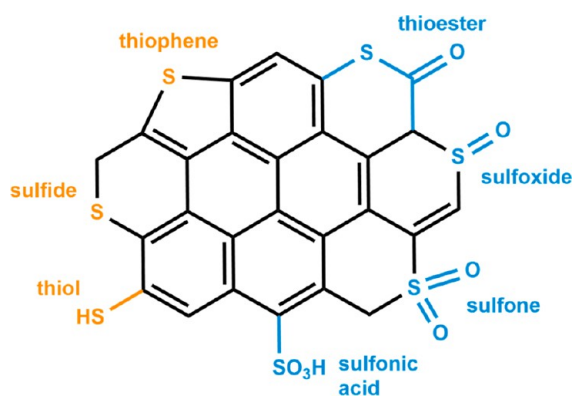


Figure 14. Structures of various prominent S species (orange) and mixed S/O species (blue) present on S-doped carbon.

carbon samples and the facile oxidation of reduced sulfur. In this sense, reduced sulfur species are oxidized by oxygen surface groups or their corresponding decomposition products before or after desorption.^{82,84} However, it should be noted that profound information on possible side reactions during the TPD analysis of S species on carbon is scarce, indicating that less attention has been paid to this issue compared to the identification and quantification of O or N species on carbon.

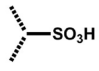
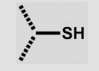
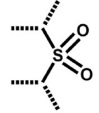
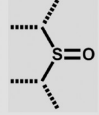
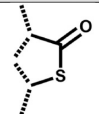
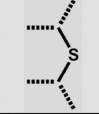
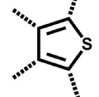
3.2. Characterization of Defect Sites. The reactivity of a carbon material is governed to a great extent by the amount and nature of its defects. For instance, the affinity of edge sites of graphitic basal planes toward the chemisorption of molecular oxygen was determined to be orders of magnitude higher than the reactivity of the basal plane itself.⁹⁰ In this context, regarding sp^2 -hybridized carbons, the term “defect” refers in principle to every deviation from the ideal stack of graphene sheets, such as differences in the binding situation of the carbon atoms, including edge sites or in-plane vacancies, and deviations from the ideal trigonal planar binding geometry, such as five- or seven-membered carbon rings or curvature.

The recognition of the high affinity of molecular oxygen toward chemisorption at unsaturated carbon sites lead to the introduction of the concept of “active surface area” (ASA) as a quantitative measure for the defect density of a carbon material, which is defined as the surface area susceptible to O_2 chemisorption.^{90–93} This active surface area can be determined by contacting a carbon surface with oxygen at a specific temperature (usually around 300 °C) that is high enough to quickly achieve equilibrium but low enough to avoid carbon gasification. The amount of chemisorbed O_2 is determined subsequently by TPD, and the active surface area is then calculated by considering the area occupation of an assumed carbon surface oxide. Initially, it was thought that carbon exhibited only two chemisorption sites, one featuring a low activation energy for O_2 chemisorption (carbon edge sites that constitute the active surface area) and another featuring a high activation energy (basal planes).⁹⁴ However, today it is accepted that a wide range of chemisorption (defect) sites are usually present in carbon materials, exhibiting a distribution of reactivity toward the chemisorption of oxygen. This reactivity range extends from intact, perfectly ordered graphitic basal planes over less-ordered graphitic domains all the way to highly reactive species that have been found to terminate edge sites such as carbenes or carbynes.^{95,96} This diversity in reactivity is also reflected by the studies of Sendt and Haynes, who examined the mechanism of O_2 chemisorption on different carbon edge sites in detail via DFT.^{97–100}

The area occupation of a carbon surface oxide that is used to calculate the ASA from the amount of desorbed oxygen is usually assumed to be identical to the area occupation of an edge carbon atom lying in the (100) plane, which corresponds to 0.083 nm².^{90,101} This assumption is of course rather simplistic, as on one hand it reflects the early conviction that there is only one participating chemisorption site (graphene edge sites) and on the other hand ignores the structural and stoichiometric ($C_1O_{0.5-2}$) complexity of the various known carbon surface oxides.

The ASA of a carbon material is usually (with few exceptions) quite small, often accounting for less than 5% of the total surface area, and differs fundamentally for various carbon materials (Table 4).^{90,102} For example, Radović et al. determined the ASA of a pyrolyzed coal sample to be 36% (of the total surface area), while the ASA of a graphitized carbon

Table 3. Decomposition Products and Desorption Temperatures of Various S Species on Carbon during Temperature-Programmed Desorption

Sulfur species	Decomposition product(s)	Desorption temperature	Carbon material	Reference
Sulfonic acids 	SO ₂	270 °C	AC ¹	[81]
	SO ₂	361 °C	AC ²	[82]
	SO ₂	227–377 °C	AC ³	[83]
	SO ₂	277 °C	AC ³	[79]
	SO ₂	<220 °C	PDC ⁴	[84,85]
	SO ₂ , SCO	270 °C	PDC ⁴	[70]
	SO ₂	250 °C	PDC ⁴	[86]
	SO ₂	230–330 °C	CNF ⁵	[87]
Thiols 		319 °C	AC ²	[82]
	SO ₂	277 °C	AC ³	[79]
	SO ₂	227–377 °C	AC ³	[83]
		<220 °C	PDC ⁴	[84,85]
		330 °C	AC ⁷	[88]
Sulfones 	SO ₂	415 °C	AC ²	[82]
	SO ₂	270 °C	PDC ⁴	[84]
	SO ₂ , SCO	270 °C	PDC ⁴	[70]
	SO ₂	270 °C	PDC ⁴	[86]
	SO ₂	500–600 °C	AC ⁷	[88]
Sulfoxides 	SO ₂	650 °C	AC ¹	[81]
	SO ₂	415 °C	AC ²	[82]
	SO ₂	350–620 °C	PDC ⁴	[84]
	SO ₂ , SCO	270 °C	PDC ⁴	[70]
	SO ₂	270 °C	PDC ⁴	[86]
Thioester 	SO ₂	350–620 °C	PDC ⁴	[84]
	-	>1000 °C	PDC ⁸	[74]
	SCO	350	PDC ⁴	[70]
Sulfides 	SO ₂	350–620 °C	PDC ⁴	[84]
	-	>1000 °C	PDC ⁸	[74]
Thiophenes 	CS, SO ₂	800–900 °C	PDC ⁴	[86]
	SO ₂	>600 °C	PDC ⁴	[85]

¹Wood-based activated carbon (BAX, Mead-Westvaco) treated with H₂S at 650 or 800 °C. ²De-ashed activated carbon (D43/1, Carbotech) modified with fuming H₂SO₄. ³Activated carbon (Norit ROX 0.8) treated with 5–18 M H₂SO₄ at 80–150 °C. ⁴Nanoporous carbon derived from poly(sodium 4-styrenesulfonate), premixed with various amounts of graphene oxide prior to carbonization. ⁵CNF sulfonated with VO²⁺/H₂SO₄ or concentrated H₂SO₄. ⁶Multiwalled CNTs treated with concentrated H₂SO₄ or a 1:3 v/v mixture of HNO₃ and H₂SO₄. ⁷CO₂-activated coal treated with H₂S at 800 °C. ⁸Mesoporous polymer-derived carbon prepared by the pyrolysis of a co-condensate of resorcinol and 4,4'-thiodiphenol with formaldehyde.

black was found to be 1.5% of the total surface area.⁹¹ These differences in ASA are closely connected with the wide variation of crystallite sizes in carbon materials, reaching from activated carbons with crystallite sizes around 1 nm at one end of the spectrum to graphite exhibiting crystallite sizes of several hundred nanometers on the opposite end. In this context, there is of course evidence for a connection between the synthesis temperature of a carbon material and its active surface area, meaning that high-temperature treatments usually

lead to an increase in structural order, which is achieved by the annealing of defect sites, and thus a decrease in the ASA. On the other hand, the crystallite orientation plays a significant role, meaning that a basal plain orientation parallel to the carbon surface is much less favorable for O₂ chemisorption than an orthogonal orientation. In this context, it is important to note that a significant fraction of relevant sp²-hybridized carbon materials are polycrystalline. This results in surfaces exhibiting a considerable degree of heterogeneity in terms of

Table 4. Ratio of (Total) Specific Surface Area to the Active Surface Area Determined by Oxygen Chemisorption and Subsequent TPD Analysis for Selected Carbon Materials

carbon material	heat treatment ¹ [°C]	SSA [m ² g ⁻¹]	ASA [% SSA]	ref
graphitized carbon black	2700	82	1.2	94
	2800	75	0.3	90
		63	<1.6	91
saran char		1224	4.1	91
graphite		1.8	<5.6	91
pyrolyzed coal	1000	630	35.7	91
	1000	50	60	101
activated carbon		1210	1.9	104
		480	5.0	104
		860	3.2	104
pyrolytic carbon ²	825	66	100	105
polymer-derived carbon ³	1000	100	80	101

¹Refers to the maximum temperature the carbon material was subjected to prior analysis of the active surface area. ²Thin carbon films obtained from CH₄ pyrolysis at 825 °C that were analyzed without being exposed to ambient atmosphere. ³Vinylidene chloride–acrylonitrile copolymer.

which fraction of the surface is represented by which particular crystal plane, thereby defining the oxygen chemisorption capacity and thus the size of the active surface area.^{102,103}

Beyond quantitative defect analysis within the concept of active surface area, efforts have also been directed at a combined qualitative and quantitative analysis of carbon edge sites, where the O₂ chemisorption step at elevated temperatures was avoided in order to gain information on the “pristine” state of defects in carbon materials. Regarding nonheteroatom-doped sp²-hybridized carbons, edge sites of individual carbon sheets are mostly occupied by hydrogen in addition to chemisorbed oxygen. However, there is also compelling evidence for the presence of nonterminated sites, which are believed to be present in form of carbynes at arm-chair edges and as carbenes at zigzag edges.¹⁰⁶

While it remains challenging to quantify the amount of nonterminated sites, high-temperature TPD has been utilized for the accurate determination of the amount of edge sites

terminated by surface oxides and hydrogen. Peak temperatures of up to 1800 °C have to be employed for this purpose, since the desorption of nonprotic hydrogen atoms in form of H₂ does not commence below 900 °C. However, even at a TPD peak temperature of 1800 °C, some hydrogen appears to remain on the carbon surface (Figure 15).¹⁰⁷ According to Ishii et al., the identification and quantification of surface oxides is also necessary to determine the total amount of edge sites, as shown in the following equation (eq 1):^{107–109}

$$N_{\text{edge}} = \text{non-terminated sites} + \text{H} + \text{carbonyl} + \text{ether} + 2\text{anhydride} + 2\text{lactone} \quad (1)$$

Surface oxides such as hydroxyl groups or carboxylic acids contain both hydrogen and oxygen but occupy a single site and are therefore included in the total amount of H emitted. An estimation of the amount of nonterminated edge sites can be attempted by measuring the magnetic susceptibility, for example; all other values can be accessed by analyzing the TPD data.¹⁰⁸

Under the assumption of a specific graphene sheet geometry, the amount of defect sites can be utilized to estimate the dimension of graphite crystallites in the examined carbon material. However, in the case of polymer-derived carbons with crystallite sizes $L_a < 100$ nm (determined by TEM), it was shown that the diameter of graphene sheets, determined by the number of edge sites, was significantly larger compared to the crystallite sizes determined by other methods. The authors note that in the case of the polymer-derived carbons the graphene sheets showed a high degree of disorder in the form of curvature, which on one hand rendered the determination of the true sheet size by methods such as XRD or TEM a challenge and on the other hand called the applicability of the utilized model geometry (coronene-based) into question.¹⁰⁸ Nevertheless, in case of natural graphite, the edge site-derived graphene sheet dimension did correspond well with the average particle size along the flat parts of the plate-like graphite particles, since the assumption of defect-free (in this case meaning nondistorted) carbon layers held true.¹⁰⁷

3.3. Characterization of Acid and Base Properties.

3.3.1. Acidity. A popular method of evaluating the amount and strength of acidic surface sites on various materials is the

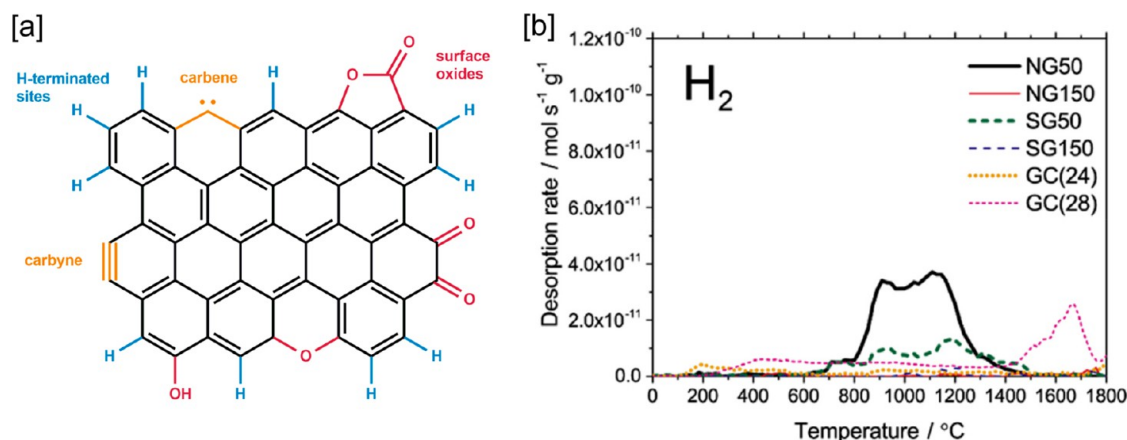


Figure 15. [a] Model of graphene edge site termination in non-heteroatom-doped carbons. [b] TPD H₂ evolution profiles of natural graphite (NG) and synthetic graphite (SG), each of which was sieved into two particle size fractions of 50 and 150 μm as well as Gilsonite coke (GC) graphitized by heat treatments at 2400 and 2800 °C (heating rate of 10 °C min⁻¹, 2 × 10⁻⁵ Pa, 40–70 mg sample, performed in an induction furnace). Reprinted with permission from ref 107. Copyright 2017 Elsevier.

temperature-programmed desorption of ammonia.^{110,111} In short, the sample is loaded with ammonia at a low temperature (usually close to room temperature) at which ammonia is chemisorbed by acidic surface sites. After being purged with inert gas, the sample is heated at a constant rate, and ammonia desorption is monitored by either determining the mass loss of the sample in a thermogravimetric balance or analyzing the effluent gas. The temperature of ammonia desorption is governed by the acidic strength of the corresponding surface species, where the amount of desorbed ammonia represents the quantity of the respective (accessible) acid centers. Ammonia is a popular probe molecule in this context because its comparatively small kinetic diameter (0.26 nm)¹¹² facilitates its access to even micropores; simultaneously, it represents a strong base that interacts with Brønsted sites as well as with Lewis sites and exhibits a wide range of adsorption enthalpies depending on the acidic strength of the studied surface site. However, for this method to be usable without restrictions, a strong adsorption of NH₃ at nonacidic sites has to be excluded.

Considering carbon materials, it is well-documented that ammonia shows little affinity for defect-free basal planes of graphite or carbon nanotubes, with the heat of adsorption calculated by DFT studies being close to zero.¹¹³ Defects in the basal plane, such as missing C atoms, increase the enthalpy of adsorption but only to 16 kJ mol⁻¹, which falls within the range of comparatively weak physisorption.¹¹⁴ For single-wall carbon nanotubes, FTIR studies have shown that no ammonia adsorption takes place, even at temperatures as low as -179 °C.¹¹⁴ Although this proves that ammonia does not show pronounced interactions with heteroatom-free crystalline carbons such as CNTs and graphite, much higher adsorption enthalpies are expected for microporous carbons in particular due to confinement effects. Accordingly, porous carbon materials such as activated carbons are widely applied as adsorbents in NH₃-capture processes.^{115,116} In this context, Domingo-García et al. showed that a substantial amount of ammonia did not desorb at temperatures of up to 300 °C even in absence of significant amounts of surface functional groups. This behavior was attributed by the authors to the texture of the studied activated carbons, which contained micropores with dimensions close to the molecular size of ammonia, leading to a significant increase in the enthalpy of adsorption.⁴⁶ Nevertheless, the quantity of chemisorbed NH₃ is substantially higher in the presence of heteroatom surface groups, and various groups have studied the surface acidity of oxidized, sulfonated, or phosphorylated carbon materials via ammonia TPD.^{46,56,117–119} Szymański et al. studied the surface acidity of a HNO₃-oxidized activated carbon and observed three distinct ammonia desorption peaks at 140, 287, and 420 °C (Figure 16). The low-temperature desorption maximum is the most pronounced and is attributed to primary adsorption sites that interact with NH₃ via hydrogen bonds. The ammonia desorption maxima at 287 and 420 °C coincided with CO₂ evolution during TPD in the absence of ammonia and were assigned to the desorption of NH₃ from ammonium carboxylate species.⁵⁶

The shape of the NH₃ desorption profile described by Szymański et al. appears to be characteristic for HNO₃ oxidized carbon materials, since similar ammonia emission profiles were observed for nitric acid-treated MWCNTs by other authors.^{120,121} Oliveira et al. examined sulfonated MWCNTs treated with concentrated H₂SO₄ at temperatures between 150 and 280 °C via ammonia TPD and observed up

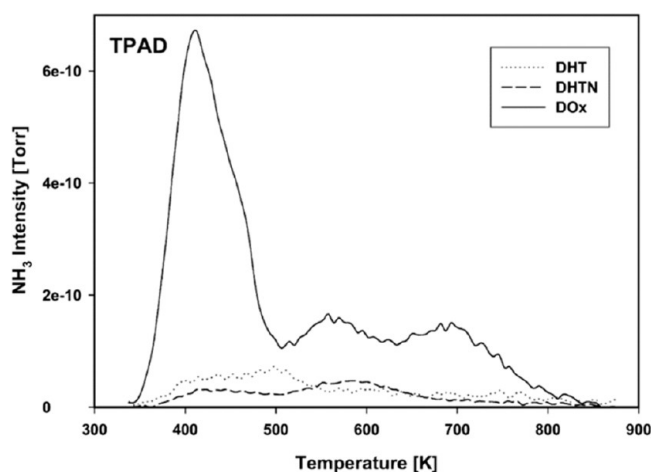


Figure 16. NH₃-TPD profiles for samples of an activated carbon subjected to thermal annealing at 750 °C (DHT), thermal annealing at 750 °C followed by an ammonia treatment at 900 °C (DHTN), and oxidation in concentrated HNO₃ at 80 °C (DOx). Reprinted with permission from ref 56. Copyright 2004 Elsevier.

to five acidic species with different acidic strengths that were responsible for NH₃ desorption between 100 and 600 °C.¹²² However, these results for sulfonated carbon materials represent a certain dissonance, since the highest proposed desorption temperature for sulfonic acid species (400 °C, see section 3.1.4) is located at least 200 °C below the highest observed NH₃ evolution, hinting at the possible involvement of side reactions.^{122,123} Beyond the comparison of desorption temperatures, the strength of the interaction between NH₃ and carbon surfaces can be described by the heat of desorption, which was for example determined by Kirilin et al., who analyzed several NH₃-TPD experiments with varying heating rates.¹²⁴

In general, it should be noted that the annealing of oxidized carbon in the presence of ammonia is a popular approach for N doping of carbon materials.^{30,33,125,126} In this context, N species formed by interaction of NH₃ with acidic sites such as carboxylic acids and anhydrides are prone to follow a cascade of transformations at higher temperatures, yielding functional groups that are on one hand increasingly temperature-stable and on the other hand might not emit NH₃ upon decomposition (Figure 12, Table 2). FTIR studies on NH₃ adsorption on oxidized carbon materials directly demonstrated the ammonolysis of carboxylic anhydrides, which yielded amides in a first step and subsequently, as a product of dehydration, imides.^{52,127} The interpretation of NH₃ TPD desorption profiles thus has to be handled with caution, since not all adsorbed NH₃ might be recovered. Additionally, the adducts of acidic chemisorption sites and ammonia might not be temperature-stable and may form other functional groups before emitting NH₃ or other N-containing volatiles. Consequently, the temperature of NH₃ desorption might not be a direct reflection of the acidic strength of a specific acidic site, and the quantity of desorbed NH₃ at a specific temperature might not reflect the concentration of the corresponding site originally present on the carbon surface.

3.3.2. Basicity. Considering the evaluation of the strength and number of basic sites via temperature programmed desorption, one of the most popular molecular probes is CO₂.^{128,129} As a comparatively small molecule (kinetic diameter of 3.3 nm),¹¹² CO₂ is able to penetrate even narrow

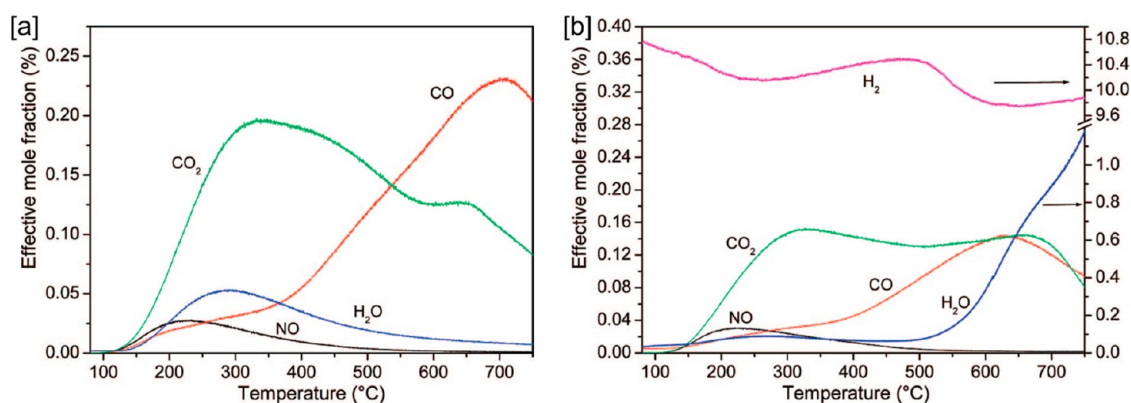


Figure 17. Comparison of the [a] TPD and [b] TPR emission profiles of MWCNTs refluxed in 65 wt % HNO₃ (plug flow setup, heating rate of 10 °C min⁻¹, total volume flow of 50 mL min⁻¹ He in case of TPD, 80 mL min⁻¹ of 10 vol % H₂ in He in case of TPR, 200 mg of MWCNT). Reprinted with permission from ref 29. Copyright 2008 American Chemical Society.

pore systems, is noncorrosive, and interacts selectively with Lewis bases on the surfaces of materials. However, the utilization of CO₂ as a molecular probe for assessing carbon surfaces has only been reported in exceptional cases, since the presence of carbon surface oxides leads to overlapping emission from CO₂ adsorbed on basic surface sites and CO₂ evolved by the thermal decomposition of oxygen surface functionalities.^{123,130,131} A possible circumvention of this problem might be provided by performing TPD experiments without the probe in an inert atmosphere in order to gain information on the CO₂ emission caused solely by thermal decomposition of surface oxides and then subtracting this emission profile from the CO₂ TPD data.¹²³

Beyond CO₂, other potential probe molecules for the evaluation of carbon surface basicity include SO₂ and HCl. In case of SO₂, there is considerable evidence in the literature that basic surface oxides (such as pyrones) or nitrogen species (such as pyridinic, pyrrolic, or quaternary N) significantly enhance the sorption capacity and strength of SO₂ on carbon adsorbents.^{132–134} However, in addition to SO₂ being highly corrosive to analytical equipment, its selectivity for specific adsorption sites is still largely unknown, impeding the effective utilization of SO₂ as a molecular probe for carbon surface basicity. Similarly, it has been shown that basic N species increase the adsorption capacity and strength of carbon materials of HCl,^{135–137} however, in this case, HCl being a potent corrosive for the analytical equipment used and a lack of systematic studies concerning the selectivity of HCl adsorption to specific surface sites also hamper the use of HCl as a molecular probe for carbon surface basicity.

4. TEMPERATURE-PROGRAMMED REDUCTION

4.1. Carbon Hydrogasification. If carbon is exposed to hydrogen at increasing temperatures (>700 °C), not only heteroatom surface groups will be hydrogenated but also the carbon matrix itself. There are major analogies to oxidative carbon gasification (e.g., with oxygen), since hydrogasification also proceeds via a two-step mechanism involving hydrogen chemisorption on carbon active sites followed by the desorption of lower hydrocarbons as reaction products.¹³⁸ However, it has to be emphasized that the reaction is equilibrium-limited, meaning that hydrocarbon (e.g., methane) formation becomes increasingly unfavorable as the temperature increases and the hydrogen partial pressure decreases.¹³⁹ In consequence, it should be noted that most “pure” carbons are

quite stable toward hydrogen at elevated temperatures and atmospheric pressure.

It is understood that the active surface area for hydrogen chemisorption defines the reactivity of a given carbon material toward hydrogasification but usually represents merely a fraction of the total surface area of the carbon material.¹⁴⁰ In this context, chemisorption takes place preferably at carbon defect sites, such as edge sites, dislocations, etc.; consequently, defect-rich carbon materials (with a high active surface area) display higher reactivities toward hydrogasification than long-range ordered crystalline carbons.¹⁴¹ At defect sites, –CH– units are consecutively converted by hydrogen chemisorption to –CH₂– and –CH₃ groups, with C–C bond cleavage and CH₄ desorption representing the final steps.¹³⁸ The extent to which dihydrogen chemisorption at neighboring carbon active sites or atomic hydrogen chemisorption drives the reaction is probably dependent on the applied temperature regime but is still not fully understood. The rate-determining step was found to be the final C–C bond cleavage, which enables hydrocarbon desorption.¹³⁹ As indicated before, the main reaction product of carbon hydrogasification is methane; however, depending on the temperature, higher hydrocarbons such as ethene, ethane, and acetylene have also been observed, all of which are believed to be primary products of carbon gasification.^{140,142}

The presence of oxygen surface complexes and base or alkali metal impurities is known to considerably accelerate the rate of carbon hydrogasification. In the case of oxygen surface groups, the higher reactivity appears to stem from nascent carbon sites, which are created by the desorption of surface oxides during the heating to temperatures required for hydrogasification.^{140,143,144} Regarding metal impurities, a considerable share of the alkali, base, and platinum group metals act as catalysts in carbon hydrogasification. The most prominent examples include Na and K as alkali metals;^{145,146} Fe, Co, and Ni as base metals;^{146–148} and Pt and Ru as platinum-group metals.^{139,149} In the case of base and platinum-group metals, the mechanism is believed to be based on metal nanoparticles migrating through the carbon matrix and “dissolving” the carbon structure along their path. Dissolved carbon species are transported on the metal surface and consecutively hydrogenated to methane on the surface of the metal nanoparticles.¹⁴⁹ Other conceivable mechanisms such as spillover of atomic hydrogen from the metal to the carbon surface appear to play minor roles in carbon hydrogasification.¹³⁹ Trivially, this influence of metals on TPR experiments has to be taken

into account, especially when carbon supported metal-based catalysts or similar materials are the subject of investigation.

4.2. Oxygen Surface Groups. If oxygen surface groups are subjected to a heating ramp in atmospheres containing hydrogen, desorption due to thermal decomposition is superimposed with the interaction of hydrogen with the carbon surface, thus promising additional information (compared to TPD) at the price of increased complexity. In this context, TPR as a method of characterizing oxygen surface groups is still in its infancy, with some studies^{150,151} performing TPR of oxidized carbon but focusing mainly on other subjects; only a few studies, e.g., those by Kundu et al.²⁹ and Calo et al.,¹⁵² have systematically explored the topic (Figure 17).

The reactivity of H₂ increases with the temperature, meaning that the low-temperature part of the TPR profile of oxidized carbon materials remains in large parts identical to the TPD profile, with significant influence of H₂ becoming visible only at higher temperatures. This reactivity threshold can be directly observed in the form of the H₂ consumption profile, which normally exhibits only minor contributions at temperatures below 500 °C but shows significant hydrogen consumption above this temperature.^{29,152,153} As a direct consequence of this reactivity threshold, the CO₂ evolution profile remains comparatively unaffected by the presence of H₂, with the total amount of desorbed CO₂ during TPR often resembling the amount detected during TPD.¹⁵² However, minor differences in the TPD and TPR CO₂ evolution profiles are usually observed and attributed to the direct hydrogenation of a minor fraction of the carboxylic acid derivatives and the generally lower thermal stability of surface oxides in the presence of H₂.^{29,152} The origin of this lower thermal stability of surface oxides remains somewhat opaque, although this might represent an indication that thermal desorption may proceed via deviant mechanisms in presence of hydrogen.^{29,152} In contrast to the CO₂ emission profile, the CO evolution profile is affected much more by the presence of H₂; the amount of CO evolution during TPR is significantly lower than that detected during TPD, with the whole CO emission profile appearing to be displaced to lower temperatures.^{29,152,153} In this context, the lower CO evolution is usually attributed to the direct reduction of CO-evolving groups under the formation of H₂O, which is enabled by the availability of a large fraction of the temperature-stable CO-evolving groups that remain on the surface even at high temperatures, i.e., when the reactivity of H₂ is sufficient for their direct hydrogenation.^{29,152,153} In addition to the direct hydrogenation of CO-emitting groups, the shift of the CO emission profile to lower temperatures appears to be the consequence of two further mechanisms. One mechanism involves the partial reduction of highly temperature-stable groups (e.g., carbonyl groups) to surface oxides of somewhat lower stability (e.g., hydroxyl groups), which overall leads to a higher CO evolution at lower temperatures.²⁹ In the second mechanism, H₂ tends to undergo chemisorption at reactive nascent carbon sites generated upon the desorption of surface oxides, which significantly decreases the probability of readsorption of gaseous carbon oxides and contributes to the shift of the CO emission profile to lower temperatures.^{52,153} The direct reduction of CO-evolving surface oxides is usually also reflected in the H₂O emission profile, which exhibits the typical low-temperature maximum corresponding to condensation reactions. However, in the presence of H₂, the profile also contains a larger contribution at high temperatures, with

an onset >550 °C that often directly coincides with the maximum of H₂ consumption.^{29,152}

4.3. Nitrogen Surface Groups. Analogous to the characterization of surface oxides, the examination of nitrogen surface groups utilizing TPR is still in its infancy. A few publications^{151,154} have touched on the subject, but only Xiao et al.⁶⁰ have conducted an in-depth study (Figure 18).

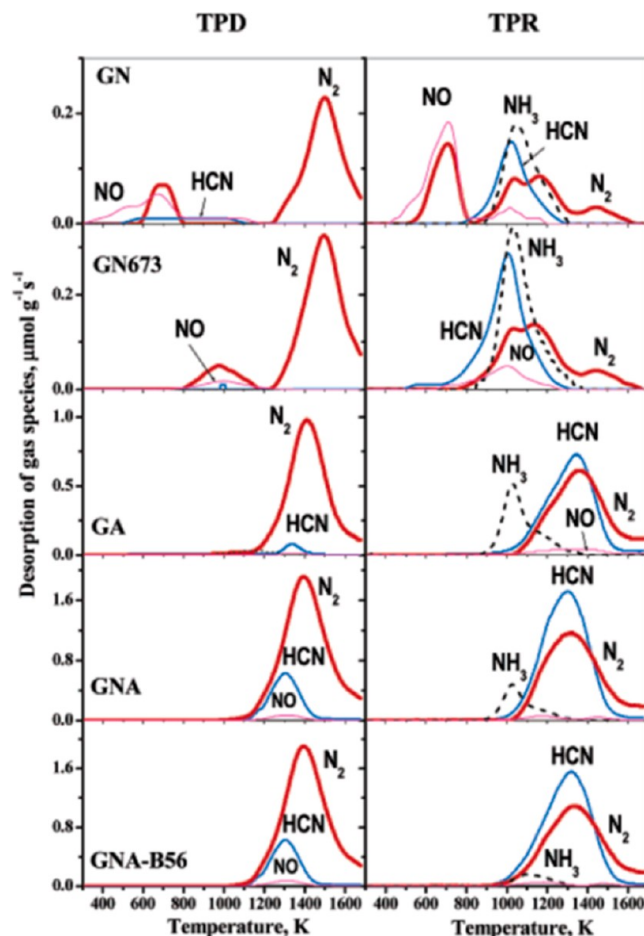
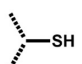
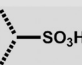
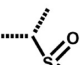
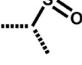

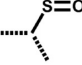


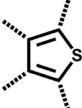


Figure 18. Comparison of the TPD and TPR emission profiles of various N-doped carbons: GN, activated carbon treated with HNO₃; GN673, GN treated at 400 °C under an inert atmosphere; GA, activated carbon treated at 800 °C in ammonia; GNA, GN treated at 800 °C in ammonia; and GNA-B56, GNA partially gasified with 20% O₂ in Ar to a burnoff of 56% (5 mg of sample, heating rate of 30 °C min⁻¹, and total volume flow of 10 mL min⁻¹). Reprinted with permission from ref 60. Copyright 2005 American Chemical Society.

The authors performed high-temperature TPD and TPR experiments to up to 1400 °C with various N-doped carbons derived from different precursors in order to compare the corresponding emission profiles that were detected by mass spectrometry. In general, the overall amount of N desorbed during TPR did not deviate considerably from the amount emitted during TPD. However, the presence of hydrogen leads to an increase in the emission of hydrogen-containing N-species such as NH₃ or HCN along with a reduction in N₂ evolution. This shift in decomposition products was assigned to the abundance of surface H-species during TPR, which appeared to alter the decomposition pathways by increasing the probability for the desorption of hydrogenated N-species.⁶⁰ Simultaneously, the NH₃ and HCN emission maxima were

Table 5. Decomposition Products and Temperatures of Various S Species during Temperature-Programmed Reduction

Sulfur species	Decomposition product(s)	Decomposition temperature	Carbon material	Reference
Thiols 	H ₂ S	265 – 300 °C	Coal ¹	[169]
		195 – 220 °C	Model compound ²	[165]
		180 °C ^a	Model compound ²	[165]
		80 °C	Coal ³	[156]
		190 – 200 °C	Coal ¹	[168]
Sulfonic acids 	SO ₂	200 – 300 °C	Coal	[167]
		300 °C	Model compound ⁴	[164]
Aliphatic Sulfones 	SO ₂ H ₂ S	600 °C	Coal	[167]
		540 °C	Model material ⁵	[163]
Aromatic Sulfones 	SO ₂ H ₂ S	600 °C	Coal	[167]
		650 °C	Model material ⁶	[163]
Aliphatic Sulfoxides 	SO H ₂ S	600 °C	Coal	[167]
		505 °C	Model compound ⁷	[163]
Aromatic Sulfoxides 	SO H ₂ S	600 °C	Coal	[167]
		575 °C	Model compound ⁸	[163]
Aliphatic Sulfides 	H ₂ S	490 – 500 °C	Model material ⁹	[165]
		360 °C ^a	Model material ⁹	[165]
		245 – 440 °C	Coal ³	[156]
		280 – 400 °C ^a	Coal	[162]
Aromatic Sulfides 	H ₂ S	590 – 610 °C	Model material ¹⁰	[165]
		300 – 320 °C ^a	Model material ¹⁰	[165]
		610 °C	Coal ³	[156]
		280 – 400 °C ^a	Coal	[162]
Thiophenes 	H ₂ S	710 – 745 °C	Model material ¹¹	[165]
		480 °C ^a	Model material ¹¹	[165]
		700 – 1000 °C	Coal ³	[156]
		430 – 530 °C ^a	Coal	[155]
		450 – 520 °C ^a	Coal	[162]

^aThe experiment was performed at 150 bar. ¹Coal reduced by potassium in liquid ammonia. ²Cysteine. ³The sample was mixed with a “reducing mixture” consisting of resorcinol, pyrogallol, phenanthrene, and 9,10-dihydrophenanthrene. “Coal” refers to pristine coal and coal pyrolyzed at temperatures between 250 and 1700 °C. ⁴Dodecyl benzenesulfonic acid. ⁵*p*-Hydroxyphenyl methyl sulfone immobilized on silica. ⁶Di(*p*-hydroxyphenyl) sulfone immobilized on silica. ⁷*p*-Hydroxyphenyl methyl sulfoxide. ⁸Di(*p*-hydroxyphenyl) sulfoxide. ⁹Thioanisole immobilized on silica. ¹⁰Diphenylsulfide immobilized on silica. ¹¹Dibenzothiophene immobilized on silica.

shifted to lower temperatures. Additionally, the N₂ evolution profiles differed significantly for some of the samples, as the unimodal profiles observed during TPD turned into multimodal profiles in the presence of hydrogen.⁶⁰ However, it remains unclear whether the multimodality is a consequence of the better resolution of previously superimposed desorption maxima of different N species or whether one N species is decomposed along multiple pathways or at energetically different surface sites.

4.4. Sulfur Surface Groups. Temperature-programmed reduction has been utilized extensively to study sulfur species found in pristine and processed coals.^{155–161} A wide variety of

different types of sulfur is usually present in coal, including inorganic (pyrite, sulfates, elemental sulfur etc.) and organic sulfur species, which differ considerably in their properties. The nature and distribution of these types of sulfur determine whether and how the corresponding coal can be further processed.^{155,157,161,162} With the focus on organic sulfur species, temperature-programmed reduction in a pure hydrogen atmosphere is carried out to temperatures of up to 1000 °C in order to discriminate sulfur species according to their stability toward reduction to H₂S.^{156,157} However, as described before, TPR experiments are characterized by competition between the thermal decomposition of surface groups and

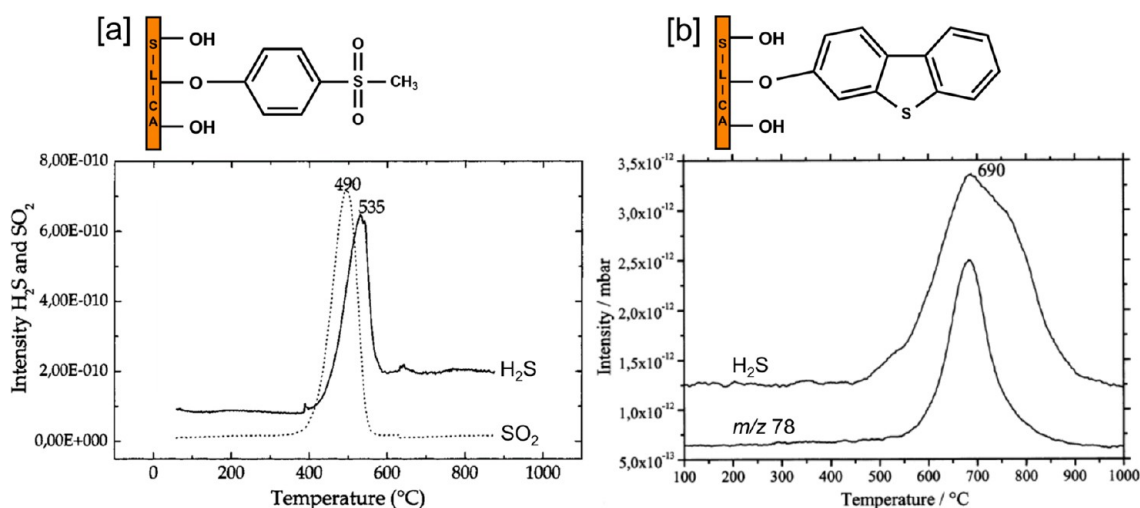


Figure 19. Temperature-programmed reduction of [a] a silica-immobilized sulfone and [b] silica-immobilized dibenzothiophene serving as reference materials for sulfur species in coal (40–100 mg of sample, plug flow reactor, heating rate of $5\text{ }^{\circ}\text{C min}^{-1}$, and total flow of 100 mL min^{-1} H_2). Panel [a] was reproduced with permission from ref 163. Copyright 2000 American Chemical Society. Panel [b] was reproduced with permission from ref 164. Copyright 2003 Elsevier.

reductive decomposition, which is mainly caused by the temperature-dependent reactivity of hydrogen. In this context, temperature-labile, highly oxidized S species such as sulfonic acids primarily decompose via thermal decomposition, consequently emitting volatile S species other than H_2S (e.g., SO_2 , SO).^{158,163,164} Since earlier setups for the examination of sulfur species in coal relied on the potentiometric detection of solely H_2S , the recovery rate of sulfur species usually did not exceed 70–90% of the total amount.^{157,158} In an attempt to increase S recovery, a high-pressure variant of TPR was introduced that applied H_2 pressures of up to 150 bar;^{155,162,165} however, considering the ambiguity of the S recovery results, mass transport limitations (high residence times), and the frequent occurrence of secondary reactions, a meaningful interpretation of high-pressure H_2S emission profiles was challenging.^{158,165}

Regarding the assignment of decomposition temperatures, most reports reach the conclusion that the stability of sulfur species on carbon toward reduction tends to follow the sequence thiophenes > aromatic sulfides \approx sulfoxides and sulfones > aliphatic sulfides > thiols and sulfonic acids (Table 5). It should be noted that some sulfur species, usually assigned as “complex” thiophenes, could not be recovered by TPR even at temperatures as high as $1000\text{ }^{\circ}\text{C}$. In order to examine the reduction and decomposition temperatures of defined sulfur species, Ismail et al.,¹⁶⁵ van Aelst et al.,¹⁶³ and Mullens et al.¹⁶⁴ conducted extensive work to establish model materials, mainly by covalently immobilizing comparatively small organic model compounds on silica (Figure 19).

Utilizing these tailor-made model materials as reference materials for TPR, it is possible to deduce precise reduction and decomposition temperatures and furthermore study potential secondary reactions (Table 5).^{158,164,165} In this context, it was found that high temperatures induce the structural evolution of aliphatic and aromatic sulfides, namely, the formation of thiophenes by cyclization and aromatization, thus considerably increasing the stability of the original species toward reduction.^{156,164} Beyond the thermally induced interconversion of sulfur species, inorganic impurities were found to obscure the results of the analysis of S compounds via

TPR.^{166,167} In particular, Ca-based minerals such as dolomite and limestone ($\text{CaCO}_3\cdot\text{MgCO}_3$ and CaCO_3 , respectively, frequently found as impurities in coals) showed a high potential for H_2S capture via the formation of CaS, leading to a significantly lower S recovery and an overall distortion of the H_2S evolution profile.¹⁶⁶

In addition to secondary reactions, the quantification of S species is usually impeded by broad H_2S emission peaks stemming from the large structural diversity of the individual classes of S species, leading to overlapping evolution maxima. In order to circumvent this challenge, deconvolution utilizing Gaussian functions has been applied to enable a meaningful quantification of S species. Beyond mathematical deconvolution, chemical modification was also carried out in order to circumvent severe signal overlap.^{168,169} The reduction of the coal with potassium in liquid ammonia was shown to be able to cleave C–S bonds of sulfides and disulfides, yielding thiols. Since thiols exhibit a decomposition temperature range that is not affected by overlap of the decomposition of other S species, this approach could be used for the quantification of aromatic or aliphatic sulfides.^{168,169}

5. TEMPERATURE-PROGRAMMED SURFACE REACTION

Even though temperature-programmed surface reaction has not been utilized extensively for the characterization of carbon materials, some studies have examined the gas-phase conversion of 2-propanol over carbon, which may serve as a potential model reaction for carbon surface characterization. However, in most cases surface characterization was not the sole purpose of those studies; all the studies used stepwise temperature changes instead of continuous heating ramps, mostly in order to be able to present steady-state conversions and selectivities as functions of temperature. The gas-phase conversion of 2-propanol in an inert atmosphere over carbon usually yields the dehydration products propene and diisopropyl ether in addition to the dehydrogenation product acetone.^{170,171} While the dehydration reactions were assigned to the presence of Brønsted acid sites, the dehydrogenation of 2-propanol to acetone was linked to Lewis acid–base pairs as

active sites.¹⁷¹ In this context, the TPSR of 2-propanol can be utilized as a model reaction to prove the presence of catalytically active and accessible Brønsted and Lewis sites by measuring the rate and selectivity of the conversion of 2-propanol to the dehydration and dehydrogenation products, respectively. In addition, carbon materials that differ in surface chemistry can be compared using the onset temperatures of the corresponding reactions in order to draw conclusions regarding the surface concentration of accessible active sites and their activities (or “strength” in the acid–base context). Szymański et al. used this model reaction to compare the surface chemistry of pristine and oxidized poly(furfuryl alcohol) derived carbon and found that the oxidized carbons exhibited a much higher dehydration activity than the pristine carbons.^{171,172} The formation of diisopropyl ether and propene was specifically assigned to the presence of carboxylic acids as Brønsted sites, while evidence was found that carboxylic acids of low acid strength were responsible for the formation of diisopropyl ether and those of higher strength were responsible for propene formation. Less obvious activity differences between oxidized and pristine carbons existed in case of the conversion of 2-propanol to acetone.¹⁷¹ Bedia et al. employed different phosphorylated biomass-derived carbons to gas-phase 2-propanol dehydration, where the onset of 2-propanol conversion could be used to compare the surface acidity of the various carbons. The dehydration activity correlated well with the overall concentration of acidic sites determined by ammonia TPD and was ascribed to the presence of surface phosphates.^{117,119}

Friedel Ortega et al. studied N-doped carbon nanotubes synthesized by the post-treatment of oxidized nanotubes with ammonia at temperatures between 300 and 700 °C, where the gas-phase conversion of 2-propanol was used specifically to characterize the acid–base properties of the carbon surface.³³ Increasing the ammonia treatment temperatures caused a significant decrease in surface acidity, with the ratio of the reaction rates of dehydrogenation and dehydration increasing considerably. In this context, the dehydration activity was assigned to acidic imide species acting as Brønsted sites, while the dehydrogenation of 2-propanol to acetone was linked to the presence of pyridinic N species. However, the authors note that, in addition to various N species, all examined materials exhibited significant concentrations of surface oxides, which could not be excluded as active sites for 2-propanol dehydration or dehydrogenation.³³ Concerning the catalytic activity, it was found that the materials treated at 300 and 700 °C with NH₃ exhibited similar 2-propanol conversion rates (although they displayed different product spectra). Interestingly, the material produced by reacting oxidized CNTs with ammonia at 500 °C was much less active even though the overall O and N content was found to be considerably higher than the material treated at 700 °C, thus hinting at the presence of a considerable amount of spectator species.³³ It should be emphasized at this point that the difficulty of interpreting the results of probe reactions will increase with the complexity of the carbon material, meaning that the surface characterization of a disordered, porous carbon that exhibits a wide range of different surface species and defects presents a significant challenge.

6. CONCLUSION AND PERSPECTIVE

Can temperature-programmed methods become the gold standard for carbon surface analysis in the future? Although

they are not yet quite up to the task, we strongly believe that every effort directed at further development of TPX techniques is worthwhile. As demand soars for reliable analytical methods for the qualitative and quantitative characterization of carbon surface species and especially for methods capable of providing information on carbon surface reactivity, TPX methods will certainly occupy key positions in future carbon surface analysis.

Considering the further development of TPX techniques, efforts directed at the understanding of the extent and mechanism of undesired side reactions would arguably promise the highest benefit for TPX as analytical methods. In this context, heat-induced transformations of surface species (e.g., the structural evolution of N species), gaseous decomposition products (e.g., CO/CO₂ interconversion via the Boudouard equilibrium) or nonselective interactions between probe molecules and the carbon surface (e.g., during NH₃ TPD) must be named as most significant issues. Furthermore, signal assignment and overlapping desorption ranges remain challenging, especially for methods such as TPR that have received comparatively little attention to date. Finally, in any case, temperature-programmed methods examine the reactivity of a given surface species, which should come into focus as one of the greatest advantages of these analytical techniques. A deeper understanding of TPX and, in this context, carbon surface reactivity can be reached by broadening the scope of investigation beyond the mere identity of a surface species and taking into account the chemical environment of a species (e.g., the “carbon backbone”), which has a significant influence on the properties of individual surface species.

With these points in mind, we would like to highlight opportunities and strategies for continuing the development of temperature programmed methods in terms of both the qualitative and quantitative assessment of carbon surface heteroatom species and the assessment of carbon reactivity.

1 In order to increase interlaboratory comparability and minimize the probability for misinterpretation, we would like to encourage the establishment of a set of “best practices” for the TPX analysis of carbon materials in general. These best practices are aimed at developing a standardized measurement and data analysis routine, within which the following aspects play decisive roles:

- The application of rigorous qualitative and quantitative off-gas analysis, meaning the identification and quantification of any constituent of the effluent gas.
- Consistent data analysis by kinetic modeling. The use of at least two different heating rates and two different inert gases (Ar or He) for every sample would pave the way for the meaningful analysis of experimental TPX data, taking into account mass transfer influences, as diffusion coefficients of gaseous reaction products are dependent on the reaction atmosphere.^{173,174}
- The development of a procedure for efficient research data management, meaning a framework for the comprehensive publication of raw experimental data, including metadata, as well as the applied data analysis procedures.

2 Concerning the further development of TPX as an analytical tool for the analysis of carbon surface heteroatom species, we would like to encourage the development of analytical standards. The availability of

carbons selectively functionalized with individual heteroatom species would provide the opportunity to tackle multiple gaps of knowledge simultaneously. For instance, side reactions such as condensation reactions of neighboring surface groups, readsorption and conversion of desorbed volatile species, and temperature-dependent structural evolution of N and S species could be comprehensively studied using selectively functionalized carbon surfaces. The examination of individual surface species on different carbon backbones acting as a “support” could clarify the influence of the chemical environment, such as the influence of carbon crystallinity on the reactivity during TPX analysis. Finally, analytical standards could be used to verify the assignment of individual surface species to decomposition products and temperature ranges (especially for TPR) and could serve as benchmarks for the kinetic modeling of TPX experiments, as proposed in the set of “best practices”. Regarding selective functionalization, initial promising work in the field of selective O,^{25,36} N,^{175,176} and S^{163,165} functionalization has been conducted, although carbon materials generated in this way have so far only been sporadically used as references in the context of TPX analysis. In the field of N- and S-doped carbons, references should be synthesized under conditions that exclude surface oxides in order to exclude mutual interference (during desorption, reduction, and structural evolution) on the TPX measurement.

- Regarding carbon reactivity, the number of defect sites available for heteroatom chemisorption plays a prominent role in a wide variety of applications of carbon materials. In this context, we would like to argue for the revival and inclusion of the concept of active surface area (ASA, see section 3.2.) in the standard repertoire of carbon surface characterization. In this sense, the active surface area, as the fraction of the total surface area available for O₂ chemisorption, could serve as a uniform and quantifiable measure of the defect density and thus the reactivity of a carbon material, which could be used to compare carbon materials for their suitability in a wide variety of applications.
- Beyond the aqueous phase, only limited approaches for assessing the surface acidity or basicity of carbon materials exist. In this sense, we would like to encourage the further development of NH₃ and CO₂ TPD for the analysis of acidic and basic centers, respectively. In order to establish NH₃ and CO₂ TPD as reliable analytical methods, considerable research effort has to be directed at clarifying the detailed interaction of NH₃ and CO₂ with individual surface species, where the elevated temperatures of the TPD procedure and thus heat-induced side reactions should be taken into account. In order to increase the selectivity for acid or base interactions, especially for the examination of acidic surface centers, molecular probes other than NH₃ might also be considered. Higher selectivity might be achieved by sterically hindered bases such as pyridine derivatives (2,6-di-*tert*-butylpyridine was already used in the selective poisoning of acidic (Brønstedt) centers on carbon-based catalysts¹⁷⁷), although the ability to penetrate pore systems is an important issue that needs to be taken into account.

5 TPSR has been used only sporadically as an analytical method for carbon materials. We would like to argue for the need to conduct a systematic assessment of the analytical potential of TPSR by investigating appropriate model reactions, such as the oxidation and dehydration of 2-propanol (with the lowest possible onset temperature) and attempting to establish clear relationships between activity and selectivity of the model reactions and the carbon surface chemistry. Despite these challenges, we believe that TPSR offers the potential to significantly complement information on the identity and quantity of a particular group using its reactivity in the context of the model reaction employed. Especially for the use of carbon materials as catalysts or as catalyst supports, this information would be a large step forward, as it takes both the chemical environment, i.e., the carbon backbone and neighboring surface species, and the accessibility of the species within the pore system into account.

■ AUTHOR INFORMATION

Corresponding Authors

Felix Herold – Faculty of Natural Sciences, Norwegian University of Science and Technology, Trondheim 7491, Norway; orcid.org/0000-0002-6430-0913; Email: felix.herold@ntnu.no

Magnus Rønning – Faculty of Natural Sciences, Norwegian University of Science and Technology, Trondheim 7491, Norway; orcid.org/0000-0002-6116-6659; Email: magnus.rønning@ntnu.no

Authors

Jan Gläsel – Department of Chemistry, Technical University of Darmstadt, Darmstadt 64287, Germany

Bastian J. M. Etzold – Department of Chemistry, Technical University of Darmstadt, Darmstadt 64287, Germany; orcid.org/0000-0001-6530-4978

Complete contact information is available at: <https://pubs.acs.org/10.1021/acs.chemmater.2c02449>

Notes

The authors declare no competing financial interest.

■ ACKNOWLEDGMENTS

F.H. acknowledges a fellowship within the Walter-Benjamin program of the Deutsche Forschungsgemeinschaft (DFG, German Research Foundation, project number 471263729) and a Career Bridging Grant from Technical University of Darmstadt. J.G. and B.E. acknowledge funding from DFG within the project ET-101/13-1.

■ REFERENCES

- Zhang, C.; Lv, W.; Tao, Y.; Yang, Q.-H. Towards superior volumetric performance: Design and preparation of novel carbon materials for energy storage. *Energy Environ. Sci.* **2015**, *8*, 1390–1403.
- Dicks, A. L. The role of carbon in fuel cells. *J. Power Sources* **2006**, *156*, 128–141.
- Salleh, W. N. W.; Ismail, A. F.; Matsuura, T.; Abdullah, M. S. Precursor Selection and Process Conditions in the Preparation of Carbon Membrane for Gas Separation: A Review. *Sep. Purif. Rev.* **2011**, *40*, 261–311.

- (4) Mohan, M.; Sharma, V.K.; Kumar, E.A.; Gayathri, V. Hydrogen storage in carbon materials—A review. *Energy Storage* **2019**, *1*, No. e35.
- (5) Sweetman, M.; May, S.; Mebberson, N.; Pendleton, P.; Vasilev, K.; Plush, S.; Hayball, J. Activated Carbon, Carbon Nanotubes and Graphene: Materials and Composites for Advanced Water Purification. *C* **2017**, *3*, 18.
- (6) Qi, W.; Su, D. Metal-Free Carbon Catalysts for Oxidative Dehydrogenation Reactions. *ACS Catal.* **2014**, *4*, 3212–3218.
- (7) Rodriguez-Reinoso, F. The role of carbon materials in heterogeneous catalysis. *Carbon* **1998**, *36*, 159–175.
- (8) Su, D. S.; Wen, G.; Wu, S.; Peng, F.; Schlögl, R. Carbocatalysis in Liquid-Phase Reactions. *Angew. Chem. Int. Ed* **2017**, *56*, 936–964.
- (9) Gerber, I. C.; Serp, P. A Theory/Experience Description of Support Effects in Carbon-Supported Catalysts. *Chem. Rev.* **2020**, *120*, 1250–1349.
- (10) Weber, A. Z.; Borup, R. L.; Darling, R. M.; Das, P. K.; Dursch, T. J.; Gu, W.; Harvey, D.; Kusoglu, A.; Litster, S.; Mench, M. M.; Mukundan, R.; Owejan, J. P.; Pharoah, J. G.; Secanell, M.; Zenyuk, I. V. A Critical Review of Modeling Transport Phenomena in Polymer-Electrolyte Fuel Cells. *J. Electrochem. Soc.* **2014**, *161*, F1254–F1299.
- (11) Etzold, B. J.; Krewer, U.; Thiele, S.; Dreizler, A.; Klemm, E.; Turek, T. Understanding the activity transport nexus in water and CO₂ electrolysis: State of the art, challenges and perspectives. *Chem. Eng. J.* **2021**, *424*, 130501.
- (12) Song, Q.; He, B.; Yao, Q.; Meng, Z.; Chen, C. Influence of Diffusion on Thermogravimetric Analysis of Carbon Black Oxidation. *Energy Fuels* **2006**, *20*, 1895–1900.
- (13) Stanmore, B. R.; Gilot, P. The influence of sample containment on the thermogravimetric measurement of carbon black reactivity. *Thermochim. Acta* **1995**, *261*, 151–164.
- (14) *Handbook of heterogeneous catalysis*, 2nd ed.; Ertl, G., Knözinger, H., Schüth, F., Weitkamp, J., Eds.; Wiley-VCH: Weinheim, Germany, 2008.
- (15) Gorgulho, H. F.; Mesquita, J. P.; Gonçalves, F.; Pereira, M. F. R.; Figueiredo, J. L. Characterization of the surface chemistry of carbon materials by potentiometric titrations and temperature-programmed desorption. *Carbon* **2008**, *46*, 1544–1555.
- (16) Figueiredo, J.; Pereira, M.; Freitas, M.; Órfão, J. Modification of the surface chemistry of activated carbons. *Carbon* **1999**, *37*, 1379–1389.
- (17) Figueiredo, J. L.; Pereira, M. F. R.; Freitas, M. M. A.; Órfão, J. J. M. Characterization of Active Sites on Carbon Catalysts. *Ind. Eng. Chem. Res.* **2007**, *46*, 4110–4115.
- (18) Otake, Y.; Jenkins, R. G. Characterization of oxygen-containing surface complexes created on a microporous carbon by air and nitric acid treatment. *Carbon* **1993**, *31*, 109–121.
- (19) Zhuang, Q.-L.; Kyotani, T.; Tomita, A. DRIFT and TK/TPD Analyses of Surface Oxygen Complexes Formed during Carbon Gasification. *Energy Fuels* **1994**, *8*, 714–718.
- (20) Zhuang, Q.-L.; Kyotani, T.; Tomita, A. The change of TPD pattern of O₂-gasified carbon upon air exposure. *Carbon* **1994**, *32*, 539–540.
- (21) Vinke, P.; van der Eijk, M.; Verbree, M.; Voskamp, A. F.; van Bekkum, H. Modification of the surfaces of a gasactivated carbon and a chemically activated carbon with nitric acid, hypochlorite, and ammonia. *Carbon* **1994**, *32*, 675–686.
- (22) Figueiredo, J. L.; Pereira, M. F. R. The role of surface chemistry in catalysis with carbons. *Catal. Today* **2010**, *150*, 2–7.
- (23) Fanning, P. E.; Vannice, M. A DRIFTS study of the formation of surface groups on carbon by oxidation. *Carbon* **1993**, *31*, 721–730.
- (24) Yan, P.; Zhang, B.; Wu, K.-H.; Su, D.; Qi, W. Surface chemistry of nanocarbon. *Carbon* **2019**, *143*, 915–936.
- (25) Herold, F.; Leubner, O.; Jeschonek, K.; Hess, C.; Drochner, A.; Qi, W.; Etzold, B. J. Methodology for the identification of carbonyl absorption maxima of carbon surface oxides in DRIFT spectra. *Carbon Trends* **2021**, *3*, 100020.
- (26) Moreno-Castilla, C.; Carrasco-Marín, F.; Mueden, A. The creation of acid carbon surfaces by treatment with (NH₄)₂S₂O₈. *Carbon* **1997**, *35*, 1619–1626.
- (27) Zielke, U.; Hüttinger, K. J.; Hoffman, W. P. Surface-oxidized carbon fibers. *Carbon* **1996**, *34*, 983–998.
- (28) Barco, G.; Maranzana, A.; Ghigo, G.; Causà, M.; Tonachini, G. The oxidized soot surface. *J. Chem. Phys.* **2006**, *125*, 194706.
- (29) Kundu, S.; Wang, Y.; Xia, W.; Muhler, M. Thermal Stability and Reducibility of Oxygen-Containing Functional Groups on Multiwalled Carbon Nanotube Surfaces. *J. Phys. Chem. C* **2008**, *112*, 16869–16878.
- (30) Kundu, S.; Xia, W.; Busser, W.; Becker, M.; Schmidt, D. A.; Havenith, M.; Muhler, M. The formation of nitrogen-containing functional groups on carbon nanotube surfaces. *Phys. Chem. Chem. Phys.* **2010**, *12*, 4351–4359.
- (31) Chernyak, S. A.; Ivanov, A. S.; Strokova, N. E.; Maslakov, K. I.; Savilov, S. V.; Lunin, V. V. Mechanism of Thermal Defunctionalization of Oxidized Carbon Nanotubes. *J. Phys. Chem. C* **2016**, *120*, 17465–17474.
- (32) Düngen, P.; Schlögl, R.; Heumann, S. Non-linear thermogravimetric mass spectrometry of carbon materials providing direct speciation separation of oxygen functional groups. *Carbon* **2018**, *130*, 614–622.
- (33) Friedel Ortega, K.; Arrigo, R.; Frank, B.; Schlögl, R.; Trunschke, A. Acid–Base Properties of N-Doped Carbon Nanotubes. *Chem. Mater.* **2016**, *28*, 6826–6839.
- (34) Marchon, B.; Carrazza, J.; Heinemann, H.; Somorjai, G. A. TPD and XPS studies of O₂, CO₂, and H₂O adsorption on clean polycrystalline graphite. *Carbon* **1988**, *26*, 507–514.
- (35) Moreno-Castilla, C.; Ferro-García, M. A.; Joly, J. P.; Bautista-Toledo, I.; Carrasco-Marín, F.; Rivera-Utrilla, J. Activated Carbon Surface Modifications by Nitric Acid, Hydrogen Peroxide, and Ammonium Peroxydisulfate Treatments. *Langmuir* **1995**, *11*, 4386–4392.
- (36) Herold, F.; Leubner, O.; Pfeifer, P.; Zakgeym, D.; Drochner, A.; Qi, W.; Etzold, B. J. Synthesis strategies towards amorphous porous carbons with selective oxygen functionalization for the application as reference material. *Carbon* **2021**, *171*, 658–670.
- (37) Rosenthal, D.; Ruta, M.; Schlögl, R.; Kiwi-Minsker, L. Combined XPS and TPD study of oxygen-functionalized carbon nanofibers grown on sintered metal fibers. *Carbon* **2010**, *48*, 1835–1843.
- (38) Hirsch, A.; Vostrowsky, O., Functionalization of Carbon Nanotubes. In *Functional Molecular Nanostructures*; Schlüter, A. D., Ed.; Topics in Current Chemistry, Vol. 245; Springer Berlin Heidelberg, Berlin, Germany, 2005; pp 193–237.
- (39) Krueger, A.; Lang, D. Functionality is Key. *Adv. Funct. Mater.* **2012**, *22*, 890–906.
- (40) Pereira, M.; Órfão, J.; Figueiredo, J. L. Oxidative dehydrogenation of ethylbenzene on activated carbon catalysts. I. Influence of surface chemical groups. *Appl. Catal., A* **1999**, *184*, 153–160.
- (41) Aksoylu, A.; Madalena, M.; Freitas, A.; Pereira, M. R.; Figueiredo, J. L. The effects of different activated carbon supports and support modifications on the properties of Pt/AC catalysts. *Carbon* **2001**, *39*, 175–185.
- (42) Zhou, J.-H.; Sui, Z.-J.; Zhu, J.; Li, P.; Chen, D.; Dai, Y.-C.; Yuan, W.-K. Characterization of surface oxygen complexes on carbon nanofibers by TPD, XPS and FT-IR. *Carbon* **2007**, *45*, 785–796.
- (43) Silva, A. M.; Machado, B. F.; Figueiredo, J. L.; Faria, J. L. Controlling the surface chemistry of carbon xerogels using HNO₃-hydrothermal oxidation. *Carbon* **2009**, *47*, 1670–1679.
- (44) Herold, F.; Prosch, S.; Oefner, N.; Brunnengräber, K.; Leubner, O.; Hermans, Y.; Hofmann, K.; Drochner, A.; Hofmann, J. P.; Qi, W.; Etzold, B. J. M. Nanoscale Hybrid Amorphous/Graphitic Carbon as Key Towards Next-Generation Carbon-Based Oxidative Dehydrogenation Catalysts. *Angew. Chem. Int. Ed* **2021**, *60*, 5898–5906.
- (45) Herold, F.; Oefner, N.; Zakgeym, D.; Drochner, A.; Qi, W.; Etzold, B. J. The High-Temperature Acidity Paradox of Oxidized

- Carbon: An in situ DRIFTS Study. *ChemCatChem* **2022**, *14*, No. e202101586.
- (46) Domingo-García, M.; López Garzón, F. J.; Pérez-Mendoza, M. J. On the characterization of chemical surface groups of carbon materials. *J. Colloid Interface Sci.* **2002**, *248*, 116–122.
- (47) Salame, I. I.; Bandosz, T. J. Surface Chemistry of Activated Carbons. *J. Colloid Interface Sci.* **2001**, *240*, 252–258.
- (48) Ishii, T.; Ozaki, J. Understanding the chemical structure of carbon edge sites by using deuterium-labeled temperature-programmed desorption technique. *Carbon* **2020**, *161*, 343–349.
- (49) Hall, P. J.; Calo, J. M. Secondary interactions upon thermal desorption of surface oxides from coal chars. *Energy Fuels* **1989**, *3*, 370–376.
- (50) Marchon, B.; Tysoe, W. T.; Carrazza, J.; Heinemann, H.; Somorjai, G. A. Reactive and kinetic properties of carbon monoxide and carbon dioxide on a graphite surface. *J. Phys. Chem.* **1988**, *92*, 5744–5749.
- (51) Li, N.; Ma, X.; Zha, Q.; Kim, K.; Chen, Y.; Song, C. Maximizing the number of oxygen-containing functional groups on activated carbon by using ammonium persulfate and improving the temperature-programmed desorption characterization of carbon surface chemistry. *Carbon* **2011**, *49*, 5002–5013.
- (52) Meldrum, B. J.; Rochester, C. H. In situ infrared study of the modification of the surface of activated carbon by ammonia, water and hydrogen. *Faraday Trans* **1990**, *86*, 1881–1884.
- (53) Wang, H.; Shao, Y.; Mei, S.; Lu, Y.; Zhang, M.; Sun, J.-K.; Matyjaszewski, K.; Antonietti, M.; Yuan, J. Polymer-Derived Heteroatom-Doped Porous Carbon Materials. *Chem. Rev.* **2020**, *120*, 9363–9419.
- (54) Rahm, M.; Hoffmann, R.; Ashcroft, N. W. Atomic and Ionic Radii of Elements 1–96. *Chem. -Eur. J.* **2016**, *22*, 14625–14632.
- (55) Mangun, C. L.; Benak, K. R.; Economy, J.; Foster, K. L. Surface chemistry, pore sizes and adsorption properties of activated carbon fibers and precursors treated with ammonia. *Carbon* **2001**, *39*, 1809–1820.
- (56) Szymański, G. S.; Grzybek, T.; Papp, H. Influence of nitrogen surface functionalities on the catalytic activity of activated carbon in low temperature SCR of NO with NH₃. *Catal. Today* **2004**, *90*, 51–59.
- (57) Arkhipova, E. A.; Ivanov, A. S.; Strokova, N. E.; Chernyak, S. A.; Shumyantsev, A. V.; Maslakov, K. I.; Savilov, S. V.; Lunin, V. V. Structural evolution of nitrogen-doped carbon nanotubes. *Carbon* **2017**, *125*, 20–31.
- (58) Jansen, R.; van Bekkum, H. Amination and ammoxidation of activated carbons. *Carbon* **1994**, *32*, 1507–1516.
- (59) Pevida, C.; Plaza, M. G.; Arias, B.; Feroso, J.; Rubiera, F.; Pis, J. J. Surface modification of activated carbons for CO₂ capture. *Appl. Surf. Sci.* **2008**, *254*, 7165–7172.
- (60) Xiao, B.; Boudou, J. P.; Thomas, K. M. Reactions of nitrogen and oxygen surface groups in nanoporous carbons under inert and reducing atmospheres. *Langmuir* **2005**, *21*, 3400–3409.
- (61) Fujisawa, K.; Tojo, T.; Muramatsu, H.; Elias, A. L.; Vega-Díaz, S. M.; Tristán-López, F.; Kim, J. H.; Hayashi, T.; Kim, Y. A.; Endo, M.; Terrones, M. Enhanced electrical conductivities of N-doped carbon nanotubes by controlled heat treatment. *Nanoscale* **2011**, *3*, 4359–4364.
- (62) Krüner, B.; Schreiber, A.; Tolosa, A.; Quade, A.; Badaczewski, F.; Pfaff, T.; Smarsly, B. M.; Presser, V. Nitrogen-containing novolac-derived carbon beads as electrode material for supercapacitors. *Carbon* **2018**, *132*, 220–231.
- (63) Boudou, J. P.; Parent, P.; Suárez-García, F.; Villar-Rodil, S.; Martínez-Alonso, A.; Tascón, J. Nitrogen in aramid-based activated carbon fibers by TPD, XPS and XANES. *Carbon* **2006**, *44*, 2452–2462.
- (64) Jia, Y. F.; Xiao, B.; Thomas, K. M. Adsorption of Metal Ions on Nitrogen Surface Functional Groups in Activated Carbons. *Langmuir* **2002**, *18*, 470–478.
- (65) Stańczyk, K.; Dziembaj, R.; Piwowarska, Z.; Witkowski, S. Transformation of nitrogen structures in carbonization of model compounds determined by XPS. *Carbon* **1995**, *33*, 1383–1392.
- (66) Favaro, M.; Perini, L.; Agnoli, S.; Durante, C.; Granozzi, G.; Gennaro, A. Electrochemical behavior of N and Ar implanted highly oriented pyrolytic graphite substrates and activity toward oxygen reduction reaction. *Electrochim. Acta* **2013**, *88*, 477–487.
- (67) Arrigo, R.; Hävecker, M.; Wrabetz, S.; Blume, R.; Lerch, M.; McGregor, J.; Parrott, E. P. J.; Zeitler, J. A.; Gladden, L. F.; Knop-Gericke, A.; Schlögl, R.; Su, D. S. Tuning the acid/base properties of nanocarbons by functionalization via amination. *J. Am. Chem. Soc.* **2010**, *132*, 9616–9630.
- (68) Arrigo, R.; Hävecker, M.; Schlögl, R.; Su, D. S. Dynamic surface rearrangement and thermal stability of nitrogen functional groups on carbon nanotubes. *Chem. Commun.* **2008**, 4891–4893.
- (69) Chambrion, P.; Orikasa, H.; Suzuki, T.; Kyotani, T.; Tomita, A. A study of the C-NO reaction by using isotopically labelled C and NO. *Fuel* **1997**, *76*, 493–498.
- (70) Seredych, M.; Bandosz, T. J. Effect of the graphene phase presence in nanoporous S-doped carbon on photoactivity in UV and visible light. *Appl. Catal., B* **2014**, *147*, 842–850.
- (71) Chin, H. Preparation and characterization of carbon-sulfur surface compounds. *Carbon* **1981**, *19*, 175–186.
- (72) Feng, W.; Kwon, S.; Feng, X.; Borguet, E.; Vidic, R. D. Sulfur Impregnation on Activated Carbon Fibers through H₂S Oxidation for Vapor Phase Mercury Removal. *J. Environ. Eng.* **2006**, *132*, 292–300.
- (73) Rai Puri, B.; Singh Hazra, R. Carbon-sulphur surface complexes on charcoal. *Carbon* **1971**, *9*, 123–134.
- (74) Zhao, X.; Zhang, Q.; Chen, C.-M.; Zhang, B.; Reiche, S.; Wang, A.; Zhang, T.; Schlögl, R.; Sheng Su, D. Aromatic sulfide, sulfoxide, and sulfone mediated mesoporous carbon monolith for use in supercapacitor. *Nano Energy* **2012**, *1*, 624–630.
- (75) Landwehr, J.; Steldinger, H.; Etzold, B. J. Introducing sulphur surface groups in microporous carbons: A mechanistic study on carbide derived carbons. *Catal. Today* **2018**, *301*, 191–195.
- (76) Schweizer, S.; Landwehr, J.; Etzold, B. J. M.; Meißner, R. H.; Amkreutz, M.; Schiffels, P.; Hill, J.-R. Combined Computational and Experimental Study on the Influence of Surface Chemistry of Carbon-Based Electrodes on Electrode–Electrolyte Interactions in Supercapacitors. *J. Phys. Chem. C* **2019**, *123*, 2716–2727.
- (77) Denis, P. A. Band gap opening of monolayer and bilayer graphene doped with aluminium, silicon, phosphorus, and sulfur. *Chem. Phys. Lett.* **2010**, *492*, 251–257.
- (78) Bak, B.; Christensen, D.; Hansen-Nygaard, L.; Rastrup-Andersen, J. The structure of thiophene. *J. Mol. Spectrosc.* **1961**, *7*, 58–63.
- (79) Gomes, H. T.; Miranda, S. M.; Sampaio, M. J.; Figueiredo, J. L.; Silva, A. M.; Faria, J. L. The role of activated carbons functionalized with thiol and sulfonic acid groups in catalytic wet peroxide oxidation. *Appl. Catal., B* **2011**, *106*, 390–397.
- (80) Rocha, R. P.; Silva, A. M.; Romero, S. M.; Pereira, M. F.; Figueiredo, J. L. The role of O- and S-containing surface groups on carbon nanotubes for the elimination of organic pollutants by catalytic wet air oxidation. *Appl. Catal., B* **2014**, *147*, 314–321.
- (81) Seredych, M.; Messali, L.; Bandosz, T. J. Analysis of factors affecting visible and UV enhanced oxidation of dibenzothiophenes on sulfur-doped activated carbons. *Carbon* **2013**, *62*, 356–364.
- (82) Terzyk, A. P. Further insights into the role of carbon surface functionalities in the mechanism of phenol adsorption. *J. Colloid Interface Sci.* **2003**, *268*, 301–329.
- (83) Gomes, H. T.; Miranda, S. M.; Sampaio, M. J.; Silva, A. M.; Faria, J. L. Activated carbons treated with sulphuric acid. *Catal. Today* **2010**, *151*, 153–158.
- (84) Seredych, M.; Singh, K.; Bandosz, T. J. Insight into the Capacitive Performance of Sulfur-Doped Nanoporous Carbons Modified by Addition of Graphene Phase. *Electroanalysis* **2014**, *26*, 109–120.

- (85) Seredych, M.; Jagiello, J.; Bandosz, T. J. Complexity of CO₂ adsorption on nanoporous sulfur-doped carbons – Is surface chemistry an important factor? *Carbon* **2014**, *74*, 207–217.
- (86) Seredych, M.; Bandosz, T. J. S-doped micro/mesoporous carbon–graphene composites as efficient supercapacitors in alkaline media. *J. Mater. Chem. A* **2013**, *1*, 11717.
- (87) Koskin, A. P.; Larichev, Y. V.; Mishakov, I. V.; Mel'gunov, M. S.; Vedyagin, A. A. Synthesis and characterization of carbon nanomaterials functionalized by direct treatment with sulfonating agents. *Microporous Mesoporous Mater.* **2020**, *299*, 110130.
- (88) Gomis-Berenguer, A.; Seredych, M.; Iniesta, J.; Lima, J. C.; Bandosz, T. J.; Ania, C. O. Sulfur-mediated photochemical energy harvesting in nanoporous carbons. *Carbon* **2016**, *104*, 253–259.
- (89) Biddinger, E. J.; Knapke, D. S.; von Deak, D.; Ozkan, U. S. Effect of sulfur as a growth promoter for CN_x nanostructures as PEM and DMFC ORR catalysts. *Appl. Catal., B* **2010**, *96*, 72–82.
- (90) Laine, N. R.; Vastola, F. J.; Walker, P. L. THE IMPORTANCE OF ACTIVE SURFACE AREA IN THE CARBON-OXYGEN REACTION. *J. Phys. Chem.* **1963**, *67*, 2030–2034.
- (91) Radović, L. R.; Walker, P. L.; Jenkins, R. G. Importance of carbon active sites in the gasification of coal chars. *Fuel* **1983**, *62*, 849–856.
- (92) Zaghbi, K.; Song, X.; Kinoshita, K. Thermal analysis of the oxidation of natural graphite. *Thermochim. Acta* **2001**, *371*, 57–64.
- (93) Ehrburger, P.; Louys, F.; Lahaye, J. The concept of active sites applied to the study of carbon reactivity. *Carbon* **1989**, *27*, 389–393.
- (94) Graham, D. Geometric Heterogeneity in the Adsorption of Nitrogen on Graphitized Carbon Surfaces. *J. Phys. Chem.* **1957**, *61*, 1310–1313.
- (95) Campbell, P.; Mitchell, R. The impact of the distributions of surface oxides and their migration on characterization of the heterogeneous carbon–oxygen reaction. *Combust. Flame* **2008**, *154*, 47–66.
- (96) Ismail, I.; Walker, P. L. Detection of low temperature carbon gasification using DSC and TGA. *Carbon* **1989**, *27*, 549–559.
- (97) Sendt, K.; Haynes, B. S. Density functional study of the reaction of O₂ with a single site on the zigzag edge of graphene. *Proc. Combust. Inst* **2011**, *33*, 1851–1858.
- (98) Sendt, K.; Haynes, B. S. Density Functional Study of the Chemisorption of O₂ Across Two Rings of the Armchair Surface of Graphite. *J. Phys. Chem. C* **2007**, *111*, 5465–5473.
- (99) Sendt, K.; Haynes, B. S. Density functional study of the chemisorption of O₂ on the armchair surface of graphite. *Proc. Combust. Inst* **2005**, *30*, 2141–2149.
- (100) Sendt, K.; Haynes, B. Density functional study of the chemisorption of O₂ on the zig-zag surface of graphite. *Combust. Flame* **2005**, *143*, 629–643.
- (101) Causton, P.; Mccanney, B. Determination of active surface areas of coal chars using a temperature-programmed desorption technique. *Fuel* **1985**, *64*, 1447–1452.
- (102) Walker, P. L.; Rusinko, F.; Austin, L. G. Gas Reactions of Carbon. *Adv. Catal.* **1959**, *11*, 133–221.
- (103) Jiang, W.; Nadeau, G.; Zaghbi, K.; Kinoshita, K. Thermal analysis of the oxidation of natural graphite — effect of particle size. *Thermochim. Acta* **2000**, *351*, 85–93.
- (104) Cheng, A.; Harriott, P. Kinetics of oxidation and chemisorption of oxygen for porous carbons with high surface area. *Carbon* **1986**, *24*, 143–150.
- (105) Tong, S. B.; Pareja, P.; Back, M. H. Correlation of the reactivity, the active surface area and the total surface area of thin films of pyrolytic carbon. *Carbon* **1982**, *20*, 191–194.
- (106) Radović, L. R.; Bockrath, B. On the chemical nature of graphene edges. *J. Am. Chem. Soc.* **2005**, *127*, S917–S927.
- (107) Ishii, T.; Kaburagi, Y.; Yoshida, A.; Hishiyama, Y.; Oka, H.; Setoyama, N.; Ozaki, J.; Kyotani, T. Analyses of trace amounts of edge sites in natural graphite, synthetic graphite and high-temperature treated coke for the understanding of their carbon molecular structures. *Carbon* **2017**, *125*, 146–155.
- (108) Ishii, T.; Kashihara, S.; Hoshikawa, Y.; Ozaki, J.; Kannari, N.; Takai, K.; Enoki, T.; Kyotani, T. A quantitative analysis of carbon edge sites and an estimation of graphene sheet size in high-temperature treated, non-porous carbons. *Carbon* **2014**, *80*, 135–145.
- (109) Matsumura, K.; Kinumoto, T.; Tsumura, T.; Toyoda, M. Evaluation of edges for carbon materials via temperature-programmed desorption and temperature-programmed oxidation. *Carbon Lett.* **2019**, *29*, 109–114.
- (110) Toba, M.; Mizukami, F.; Niwa, S.; Kiyozumi, Y.; Maeda, K.; Annala, A.; Komppa, V. Effect of preparation methods on properties of alumina/titanias. *J. Mater. Chem.* **1994**, *4*, 585.
- (111) Hidalgo, C. V.; Itoh, H.; Hattori, T.; Niwa, M.; Murakami, Y. Measurement of the acidity of various zeolites by temperature-programmed desorption of ammonia. *J. Catal.* **1984**, *85*, 362–369.
- (112) Gao, F.; Walter, E. D.; Karp, E. M.; Luo, J.; Tonkyn, R. G.; Kwak, J. H.; Szanyi, J.; Peden, C. H. Structure–activity relationships in NH₃-SCR over Cu-SSZ-13 as probed by reaction kinetics and EPR studies. *J. Catal.* **2013**, *300*, 20–29.
- (113) Bauschlicher, C. W.; Ricca, A. Binding of NH₃ to graphite and to a (9,0) carbon nanotube. *Phys. Rev. B* **2004**, *70*, 11.
- (114) Feng, X.; Irle, S.; Witek, H.; Morokuma, K.; Vidic, R.; Borguet, E. Sensitivity of ammonia interaction with single-walled carbon nanotube bundles to the presence of defect sites and functionalities. *J. Am. Chem. Soc.* **2005**, *127*, 10533–10538.
- (115) Park, S.-J.; Jin, S.-Y. Effect of ozone treatment on ammonia removal of activated carbons. *J. Colloid Interface Sci.* **2005**, *286*, 417–419.
- (116) Huang, C.-C.; Li, H.-S.; Chen, C.-H. Effect of surface acidic oxides of activated carbon on adsorption of ammonia. *J. Hazard. Mater.* **2008**, *159*, 523–527.
- (117) Bedia, J.; Ruiz-Rosas, R.; Rodríguez-Mirasol, J.; Cordero, T. A kinetic study of 2-propanol dehydration on carbon acid catalysts. *J. Catal.* **2010**, *271*, 33–42.
- (118) Fulvio, P. F.; Mayes, R. T.; Bauer, J. C.; Wang, X.; Mahurin, S. M.; Veith, G. M.; Dai, S. One-pot[®] synthesis of phosphorylated mesoporous carbon heterogeneous catalysts with tailored surface acidity. *Catal. Today* **2012**, *186*, 12–19.
- (119) Bedia, J.; Rosas, J. M.; Márquez, J.; Rodríguez-Mirasol, J.; Cordero, T. Preparation and characterization of carbon based acid catalysts for the dehydration of 2-propanol. *Carbon* **2009**, *47*, 286–294.
- (120) Xia, W.; Wang, Y.; Bergsträßer, R.; Kundu, S.; Muhler, M. Surface characterization of oxygen-functionalized multi-walled carbon nanotubes by high-resolution X-ray photoelectron spectroscopy and temperature-programmed desorption. *Appl. Surf. Sci.* **2007**, *254*, 247–250.
- (121) Li, C.; Zhao, A.; Xia, W.; Liang, C.; Muhler, M. Quantitative Studies on the Oxygen and Nitrogen Functionalization of Carbon Nanotubes Performed in the Gas Phase. *J. Phys. Chem. C* **2012**, *116*, 20930–20936.
- (122) Oliveira, B. L.; Teixeira da Silva, V. Sulfonated carbon nanotubes as catalysts for the conversion of levulinic acid into ethyl levulinate. *Catal. Today* **2014**, *234*, 257–263.
- (123) Nahavandi, M.; Kasanneni, T.; Yuan, Z. S.; Xu, C. C.; Rohani, S. Efficient Conversion of Glucose into 5-Hydroxymethylfurfural Using a Sulfonated Carbon-Based Solid Acid Catalyst: An Experimental and Numerical Study. *ACS Sustainable Chem. Eng.* **2019**, *7* (14), 11970–11984.
- (124) Kirilin, A. V.; Hasse, B.; Tokarev, A. V.; Kustov, L. M.; Baeva, G. N.; Bragina, G. O.; Stakheev, A. Y.; Rautio, A.-R.; Salmi, T.; Etzold, B. J. M.; Mikkola, J.-P.; Murzin, D. Y. Aqueous-phase reforming of xylitol over Pt/C and Pt/TiC-CDC catalysts: catalyst characterization and catalytic performance. *Catal. Sci. Technol.* **2014**, *4*, 387–401.
- (125) Ott, S.; Orfanidi, A.; Schmies, H.; Anke, B.; Nong, H. N.; Hübner, J.; Gernert, U.; Gliech, M.; Lerch, M.; Strasser, P. Ionomer distribution control in porous carbon-supported catalyst layers for high-power and low Pt-loaded proton exchange membrane fuel cells. *Nat. Mater.* **2020**, *19*, 77–85.

- (126) Schmies, H.; Hornberger, E.; Anke, B.; Jurzinsky, T.; Nong, H. N.; Dionigi, F.; Kühn, S.; Drnec, J.; Lerch, M.; Cremers, C.; Strasser, P. Impact of Carbon Support Functionalization on the Electrochemical Stability of Pt Fuel Cell Catalysts. *Chem. Mater.* **2018**, *30*, 7287–7295.
- (127) Zheng, W.; Hu, J.; Rapoport, S.; Zheng, Z.; Wang, Z.; Han, Z.; Langer, J.; Economy, J. Activated carbon fiber composites for gas phase ammonia adsorption. *Microporous Mesoporous Mater.* **2016**, *234*, 146–154.
- (128) Hong, W.-J.; Iwamoto, S.; Inoue, M. Direct NO decomposition over a Ce–Mn mixed oxide modified with alkali and alkaline earth species and CO₂-TPD behavior of the catalysts. *Catal. Today* **2011**, *164*, 489–494.
- (129) Azzouz, A.; Nistor, D.; Miron, D.; Ursu, A. V.; Sajin, T.; Monette, F.; Niquette, P.; Hausler, R. Assessment of acid–base strength distribution of ion-exchanged montmorillonites through NH₃ and CO₂-TPD measurements. *Thermochim. Acta* **2006**, *449*, 27–34.
- (130) Guo, D.; Shibuya, R.; Akiba, C.; Saji, S.; Kondo, T.; Nakamura, J. Active sites of nitrogen-doped carbon materials for oxygen reduction reaction clarified using model catalysts. *Science* **2016**, *351*, 361–365.
- (131) Chen, H.; Sun, F.; Wang, J.; Li, W.; Qiao, W.; Ling, L.; Long, D. Nitrogen Doping Effects on the Physical and Chemical Properties of Mesoporous Carbons. *J. Phys. Chem. C* **2013**, *117*, 8318–8328.
- (132) Bagreev, A.; Bashkova, S.; Bandoz, T. J. Adsorption of SO₂ on Activated Carbons. *Langmuir* **2002**, *18*, 1257–1264.
- (133) Raymundo-Piñero, E.; Cazorla-Amorós, D.; Linares-Solano, A. Temperature programmed desorption study on the mechanism of SO₂ oxidation by activated carbon and activated carbon fibres. *Carbon* **2001**, *39*, 231–242.
- (134) Davini, P. Adsorption and desorption of SO₂ on active carbon. *Carbon* **1990**, *28*, 565–571.
- (135) Wang, X.; Dai, B.; Wang, Y.; Yu, F. Nitrogen-Doped Pitch-Based Spherical Active Carbon as a Nonmetal Catalyst for Acetylene Hydrochlorination. *ChemCatChem* **2014**, *6*, 2339–2344.
- (136) Zhang, C.; Kang, L.; Zhu, M.; Dai, B. Nitrogen-doped active carbon as a metal-free catalyst for acetylene hydrochlorination. *RSC Adv.* **2015**, *5*, 7461–7468.
- (137) Zhang, T.; Zhao, J.; Xu, J.; Xu, J.; Di, X.; Li, X. Oxygen and nitrogen-doped metal-free carbon catalysts for hydrochlorination of acetylene. *Chin. J. Chem. Eng.* **2016**, *24*, 484–490.
- (138) Zielke, C. W.; Gorin, E. Kinetics of Carbon Gasification - Interaction of Hydrogen with Low Temperature Char at 1500° to 1700° F. *Ind. Eng. Chem.* **1955**, *47*, 820–825.
- (139) Holstein, W. L.; Boudart, M. Hydrogenolysis of carbon and its catalysis by platinum. *J. Catal.* **1981**, *72*, 328–337.
- (140) Blackwood, J. D.; McCarthy, D. J. The mechanism of hydrogenation of coal to methane. *Aust. J. Chem.* **1966**, *19*, 797.
- (141) Liu, X.; Zheng, Y.; Liu, Z.; Ding, H.; Huang, X.; Zheng, C. Study on the evolution of the char structure during hydrogasification process using Raman spectroscopy. *Fuel* **2015**, *157*, 97–106.
- (142) Cao, J.-R.; Back, M. H. Kinetics of the reaction of hydrogen with thin films of carbon. *Carbon* **1982**, *20*, 505–512.
- (143) Treptau, M. H.; Miller, D. J. Hydrogen gasification of HNO₃-oxidized carbons. *Carbon* **1991**, *29*, 531–539.
- (144) Menéndez, J. A.; Phillips, J.; Xia, B.; Radovic, L. R. On the Modification and Characterization of Chemical Surface Properties of Activated Carbon: In the Search of Carbons with Stable Basic Properties. *Langmuir* **1996**, *12*, 4404–4410.
- (145) Cypres, R.; Ghodsi, M.; Feron, D. Influence of added alkaline salts on hydrogenation kinetics of coal. *Thermochim. Acta* **1984**, *81*, 105–112.
- (146) Kokorotsikos, P. S.; Stavropoulos, G. G.; Sakellaropoulos, G. P. Effect of catalyst impregnation conditions on Greek lignite hydrogasification. *Fuel* **1986**, *65*, 1462–1465.
- (147) McKee, D. W. Effect of metallic impurities on the gasification of graphite in water vapor and hydrogen. *Carbon* **1974**, *12*, 453–464.
- (148) Tomita, A.; Higashiyama, K.; Tamai, Y. Scanning electron microscopic study on the catalytic gasification of coal. *Fuel* **1981**, *60*, 103–114.
- (149) Goethel, P. J.; Yang, R. T. The tunneling action of group VIII metal particles in catalyzed graphite hydrogenation. *J. Catal.* **1988**, *114*, 46–52.
- (150) Oliveira, L. C.; Silva, C. N.; Yoshida, M. I.; Lago, R. M. The effect of H₂ treatment on the activity of activated carbon for the oxidation of organic contaminants in water and the H₂O₂ decomposition. *Carbon* **2004**, *42*, 2279–2284.
- (151) Xu, N.; Zhu, M.; Zhang, J.; Zhang, H.; Dai, B. Nitrogen functional groups on an activated carbon surface to effect the ruthenium catalysts in acetylene hydrochlorination. *RSC Adv.* **2015**, *5*, 86172–86178.
- (152) Calo, J. M.; Cazorla-Amorós, D.; Linares-Solano, A.; Román-Martínez, M. C.; de Lecea, C.-M. The effects of hydrogen on thermal desorption of oxygen surface complexes. *Carbon* **1997**, *35*, 543–554.
- (153) Román-Martínez, M. C.; Cazorla-Amorós, D.; Linares-Solano, A.; de Lecea, C.-M. Tpd and TPR characterization of carbonaceous supports and Pt/C catalysts. *Carbon* **1993**, *31*, 895–902.
- (154) Liu, S.; Yang, H.; Huang, X.; Liu, L.; Cai, W.; Gao, J.; Li, X.; Zhang, T.; Huang, Y.; Liu, B. Identifying Active Sites of Nitrogen-Doped Carbon Materials for the CO₂ Reduction Reaction. *Adv. Funct. Mater.* **2018**, *28*, 1800499.
- (155) Mitchell, S. C.; Snape, C. E.; Garcia, R.; Ismail, K.; Bartle, K. D. Determination of organic sulfur forms in some coals and kerogens by high pressure temperature-programmed reduction. *Fuel* **1994**, *73*, 1159–1166.
- (156) Yperman, J.; Franco, D.; Mullens, J.; van Poucke, L. C.; Gryglewicz, G.; Jasienko, S. Determination of sulfur groups in pyrolysed low-rank coal by atmospheric-pressure t.p.r. *Fuel* **1995**, *74*, 1261–1266.
- (157) van Aelst, J.; Yperman, J.; Franco, D. V.; Mullens, J.; van Poucke, L. C.; Palmer, S. R. Sulphur distribution in Illinois no. 6 coal subjected to different oxidation pre-treatments. *Fuel* **1997**, *76*, 1377–1381.
- (158) Yperman, J.; Maes, I. I.; van den Rul, H.; Mullens, S.; van Aelst, J.; Franco, D. V.; Mullens, J.; van Poucke, L. C. Sulphur group analysis in solid matrices by atmospheric pressure-temperature programmed reduction. *Anal. Chim. Acta* **1999**, *395*, 143–155.
- (159) Kozłowski, M.; Pietrzak, R.; Wachowska, H.; Yperman, J. AP-TPR study of sulphur in coals subjected to mild oxidation. Part 1. Demineralised coals. *Fuel* **2002**, *81*, 2397–2405.
- (160) Marinov, S. P.; Tyuliev, G.; Stefanova, M.; Carleer, R.; Yperman, J. Low rank coals sulphur functionality study by AP-TPR/TPO coupled with MS and potentiometric detection and by XPS. *Fuel Process. Technol.* **2004**, *85*, 267–277.
- (161) Marinov, S. P.; Stefanova, M.; Stamenova, V.; Carleer, R.; Yperman, J. Sulphur functionality study of steam pyrolyzed “Mequinenza” lignite using reductive pyrolysis technique coupled with MS and GC/MS detection systems. *Fuel Process. Technol.* **2005**, *86*, 523–534.
- (162) Lafferty, C. J.; Mitchell, S. C.; Garcia, R.; Snape, C. E. Investigation of organic sulphur forms in coals by high pressure temperature-programmed reduction. *Fuel* **1993**, *72*, 367–371.
- (163) van Aelst, J.; Yperman, J.; Franco, D. V.; van Poucke, L. C.; Buchanan, A. C.; Britt, P. F. Study of Silica-Immobilized Sulfur Model Compounds as Calibrants for the AP-TPR Study of Oxidized Coal Samples. *Energy Fuels* **2000**, *14*, 1002–1008.
- (164) Mullens, S.; Yperman, J.; Reggers, G.; Carleer, R.; Buchanan, A.; Britt, P.; Rutkowski, P.; Gryglewicz, G. A study of the reductive pyrolysis behaviour of sulphur model compounds. *J. Anal. Appl. Pyrolysis* **2003**, *70*, 469–491.
- (165) Ismail, K.; Mitchell, S. C.; Brown, S. D.; Snape, C. E.; Buchanan, A. C.; Britt, P. F.; Franco, D. V.; Maes, I. I.; Yperman, J. Silica-Immobilized Sulfur Compounds as Solid Calibrants for Temperature-Programmed Reduction and Probes for the Thermal Behavior of Organic Sulfur Forms in Fossil Fuels. *Energy Fuels* **1995**, *9*, 707–716.

(166) Maes, I. I.; Gryglewicz, G.; Yperman, J.; Franco, D. V.; Mullens, J.; van Poucke, L. C. Effect of calcium and calcium minerals in coal on its thermal analysis. *Fuel* **1997**, *76*, 143–147.

(167) Rutkowski, P.; Mullens, S.; Yperman, J.; Gryglewicz, G. AP-TPR investigation of the effect of pyrite removal on the sulfur characterization of different rank coals. *Fuel Process. Technol.* **2002**, *76*, 121–138.

(168) Kozłowski, M.; Wachowska, H.; Yperman, J.; Franco, D. V.; Mullens, J.; van Poucke, L. C. Atmospheric-Pressure Temperature-Programmed Reduction Study of High-Sulfur Coals Reduced in a Potassium/Liquid Ammonia System. *Energy Fuels* **1998**, *12*, 1142–1147.

(169) Kozłowski, M.; Maes, I.; Wachowska, H.; Yperman, J.; Franco, D.; Mullens, J.; van Poucke, L. Reduction of high-sulphur coal in the potassium–liquid ammonia system. *Fuel* **1999**, *78*, 769–774.

(170) Grunewald, G. C.; Drago, R. S. Carbon molecular sieves as catalysts and catalyst supports. *J. Am. Chem. Soc.* **1991**, *113*, 1636–1639.

(171) Szymański, G. S.; Rychlicki, G. Catalytic conversion of propan-2-ol on carbon catalysts. *Carbon* **1993**, *31*, 247–257.

(172) Szymański, G. S.; Rychlicki, G. Catalytic conversion of 2-propanol on cation-substituted forms of oxidized carbon. *React. Kinet. Catal. Lett.* **1991**, *43*, 475–479.

(173) Heym, F.; Etzold, B. J. M.; Kern, C.; Jess, A. An improved method to measure the rate of vaporisation and thermal decomposition of high boiling organic and ionic liquids by thermogravimetric analysis. *Phys. Chem. Chem. Phys.* **2010**, *12*, 12089–12100.

(174) Heym, F.; Korth, W.; Etzold, B.; Kern, C.; Jess, A. Determination of vapor pressure and thermal decomposition using thermogravimetric analysis. *Thermochim. Acta* **2015**, *622*, 9–17.

(175) Cui, X.; Pan, Z.; Zhang, L.; Peng, H.; Zheng, G. Selective Etching of Nitrogen-Doped Carbon by Steam for Enhanced Electrochemical CO₂ Reduction. *Adv. Energy Mater.* **2017**, *7*, 1701456.

(176) Luo, Z.; Lim, S.; Tian, Z.; Shang, J.; Lai, L.; MacDonald, B.; Fu, C.; Shen, Z.; Yu, T.; Lin, J. Pyridinic N doped graphene: Synthesis, electronic structure, and electrocatalytic property. *J. Mater. Chem.* **2011**, *21*, 8038.

(177) Yan, P.; Zhang, X.; Herold, F.; Li, F.; Dai, X.; Cao, T.; Etzold, B. J. M.; Qi, W. Methanol oxidative dehydrogenation and dehydration on carbon nanotubes: Active sites and basic reaction kinetics. *Catal. Sci. Technol.* **2020**, *10*, 4952–4959.

Recommended by ACS

Insights on Carbon Neutrality by Photocatalytic Conversion of Small Molecules into Value-Added Chemicals or Fuels

Haimiao Jiao, Junwang Tang, *et al.*

NOVEMBER 04, 2022
ACCOUNTS OF MATERIALS RESEARCH

READ 

Intrinsic Carbon Defects for the Electrosynthesis of H₂O₂

Wang Wang, Shengli Chen, *et al.*

SEPTEMBER 21, 2022
THE JOURNAL OF PHYSICAL CHEMISTRY LETTERS

READ 

Chemisorption of CO₂ on Nitrogen-Doped Graphitic Carbons

Riku Shibuya, Junji Nakamura, *et al.*

NOVEMBER 15, 2022
LANGMUIR

READ 

Correlating Structural Properties with Electrochemical Behavior of Non-graphitizable Carbons in Na-Ion Batteries

Blaž Tratnik, Robert Dominko, *et al.*

AUGUST 23, 2022
ACS APPLIED ENERGY MATERIALS

READ 

Get More Suggestions >